Article No. jmbi.1999.2594 available online at http://www.idealibrary.com on IDEAL J. Mol. Biol. (1999) 287, 943–960

JMB

Studies on the Active Site of Deacetoxycephalosporin C Synthase

Matthew D. Lloyd[1]*, Hwei-Jen Lee[1], Karl Harlos[2], Zhi-Hong Zhang[1] Jack E. Baldwin[1], Christopher J. Schofield[1], John M. Charnock[3] C. David Garner[3], Takane Hara[4], Anke C. Terwisscha van Scheltinga[5] Karin Valegård[4], Jenny A. C. Viklund[4], Janos Hajdu[4], Inger Andersson[5] Åke Danielsson[6] and Rama Bhikhabhai[6]

[1]*The Dyson Perrins Laboratory and the Oxford Centre for Molecular Sciences, South Parks Road, Oxford OX1 3QY UK*

[2]*The Laboratory of Molecular Biophysics and Oxford Centre for Molecular Sciences, South Parks Road, Oxford OX1 3QU UK*

[3]*Department of Chemistry University of Manchester Manchester M13 9PL, UK*

[4]*Department of Biochemistry Uppsala University, Box 576 S-751 23 Uppsala, Sweden*

[5]*Department of Molecular Biology, Swedish University of Agricultural Sciences, P.O. Box 590, S-751 24 Uppsala, Sweden*

[6]*Amersham Pharmacia Biotech S-751 84 Uppsala, Sweden*

**Corresponding author*

The Fe(II) and 2-oxoglutarate-dependent dioxygenase deacetoxycephalosporin C synthase (DAOCS) from *Streptomyces clavuligerus* was expressed at ca 25% of total soluble protein in *Escherichia coli* and purified by an efficient large-scale procedure. Purified protein catalysed the conversions of penicillins N and G to deacetoxycephems. Gel filtration and light scattering studies showed that in solution monomeric apo-DAOCS is in equilibrium with a trimeric form from which it crystallizes. DAOCS was crystallized ±Fe(II) and/or 2-oxoglutarate using the hanging drop method. Crystals diffracted to beyond 1.3 Å resolution and belonged to the *R*3 space group (unit cell dimensions: $a = b = 106.4$ Å, $c = 71.2$ Å; $\alpha = \beta = 90°$, $\gamma = 120°$ (in the hexagonal setting)). Despite the structure revealing that Met180 is located close to the reactive oxidizing centre of DAOCS, there was no functional difference between the wild-type and selenomethionine derivatives. X-ray absorption spectroscopic studies in solution generally supported the iron co-ordination chemistry defined by the crystal structures. The Fe K-edge positions of 7121.2 and 7121.4 eV for DAOCS alone and with 2-oxoglutarate were both consistent with the presence of Fe(II). For Fe(II) in DAOCS the best fit to the Extended X-ray Absorption Fine Structure (EXAFS) associated with the Fe K-edge was found with two His imidazolate groups at 1.96 Å, three nitrogen or oxygen atoms at 2.11 Å and one other light atom at 2.04 Å. For the Fe(II) in the DAOCS-2-oxoglutarate complex the EXAFS spectrum was successfully interpreted by backscattering from two His residues (Fe-N at 1.99 Å), a bidentate *O*,*O*-co-ordinated 2-oxoglutarate with Fe-O distances of 2.08 Å, another O atom at 2.08 Å and one at 2.03 Å. Analysis of the X-ray crystal structural data suggests a binding mode for the penicillin N substrate and possible roles for the C terminus in stabilising the enzyme and ordering the reaction mechanism.

Keywords: antibiotic biosynthesis; dioxygenase; EXAFS; iron; 2-oxoglutarate

Abbreviations used: ACV, L-δ-(α-aminoadipoyl)-L-cysteinyl-D-valine; ADH, alcohol dehydrogenase; AUFS, absorbance units full scale; 7-ADCA, 7-aminodeacetoxycephalosporanic acid; 6-APA, 6-aminopenicillanic acid; D-AA, D-δ-(α-aminoadipoyl)-; BSA, bovine serum albumin; DAC, deacetylcephalosporin C; DACS, deacetylcephalosporin C synthase; DAOC, deacetoxycephalosporin C; DAOCS, deacetoxycephalosporin C synthase; DTNB, 5,5′-dithio-bis(2-nitrobenzoic acid); ESI MS, electrospray ionisation mass spectrometry; EXAFS, extended X-ray absorption fine structure; G-7-ADCA, phenylacetyl-7-aminodeacetoxycephalosporanic acid; IU, nmol/minute; L-AA, L-δ-(α-aminoadipoyl)-; N/D, not determined; PMSF, phenylmethylsulfonyl fluoride; PEI, polyethylenimine; TCA, trichloroacetic acid; TSP, 2,2′,3,3′-[$^2H_4$]trimethylsilylpropanoate, sodium salt; XAS, X-ray absorption spectroscopy; ′ denotes residues derived from a neighbouring molecule in the crystal structure.

E-mail address of the corresponding author: matthew.lloyd@chem.ox.ac.uk

0022-2836/99/150943–18 $30.00/0

Introduction

The first committed step in the biosynthesis of cephalosporins is expansion of the five-membered thiazolidine ring of penicillin N (**1**) to deacetoxycephalosporin C (DAOC, **2**), which contains the characteristic six-membered cephem ring. Subsequent hydroxylation of DAOC (**2**) leads to deacetylcephalosporin C (DAC, **3**; Figure 1). In prokaryotes, e.g. *Streptomyces clavuligerus*, the conversions of (**1**) to (**2**) and of (**2**) to (**3**) are catalysed (at least predominately) by separate enzymes, deacetoxycephalosporin C synthase (DAOCS) and deacetylcephalosporin C synthase (DACS). In eukaryotes, e.g. *Cephalosporium acremonium*, both steps are catalysed by a single, bifunctional enzyme (DAOC/DAC synthase). In *C. acremonium* DAC (**3**) is converted by acetylation into cephalosporin C, whilst in prokaryotes alternative pathways lead to other cephems, e.g. in *S. clavuligerus* DAC (**3**) is converted *via* several steps into cephamycin C (**4**) (for reviews see: Baldwin & Abraham, 1988; Baldwin & Schofield, 1992). Medicinally useful cephalosporins are produced by *in vitro* removal of the D-δ-(α-aminoadipoyl)-side-chain from a fermented cephalosporin followed by reacylation with the requisite side-chain (see e.g. Crawford *et al.*, 1995). Alternatively, useful cephems may be obtained by the chemical ring expansion of the corresponding penicillin (Morin *et al.*, 1963; Chauvette *et al.*, 1971; Colvin, 1992).

The three oxygenases involved in the conversion of penicillin N (**1**) to DAOC (**2**) and DAC (**3**) are members of the non-heme Fe(II)-dependent family of dioxygenases (Prescott, 1993; Que & Ho, 1996; Hegg & Que, 1997). Each reaction has a stoichiometric requirement for 2-oxoglutarate and (presumably) dioxygen and *in vitro* optimum substrate conversion requires the presence of DTT and ascorbate. The hydroxylation of (**2**) to give (**3**) may be regarded as a typical type of reaction catalysed by 2-oxoglutarate utilising dioxygenases, but the oxidative ring expansion of (**1**) to give (**2**) is unique. Labelling studies on the mechanism of ring expansion indicate that cleavage of the C-H bond of the β-methyl group precedes that of the C-2 C-H bond (Baldwin *et al.*, 1991) and have provided evidence for a methylene radical intermediate (Pang *et al.*, 1984; Townsend *et al.*, 1985).

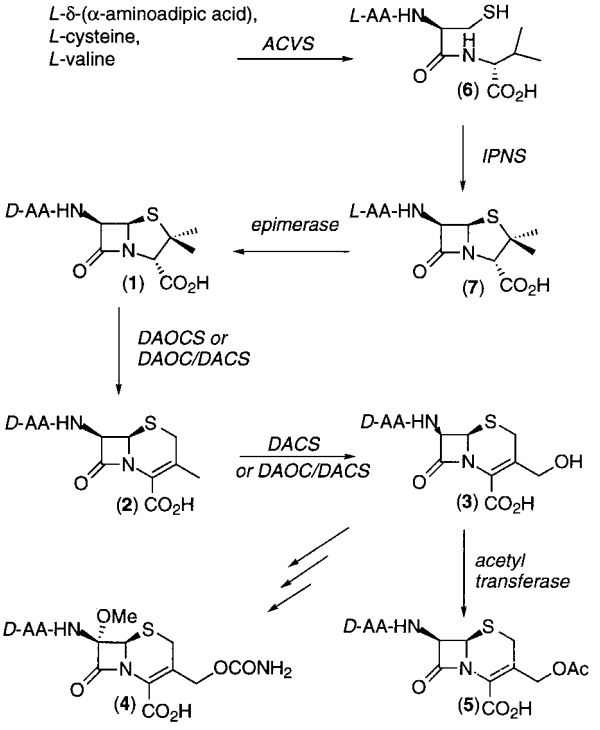

Figure 1. The biosynthesis of penicillins, cephalosporins and cephamycins (names of compounds (**1**) to (**7**) are given in the text).

Isopenicillin N synthase (IPNS), for which crystal structures have been described (Roach *et al.*, 1995, 1997), catalyses the oxidative bicyclisation of the tripeptide, L-δ-(α-aminoadipoyl)-L-cysteinyl-D-valine (ACV, **6**) to isopenicillin N (**7**), the immediate precursor of penicillin N (1) (Figure 1). IPNS does not require a 2-oxoglutarate cosubstrate since it catalyses a four-electron oxidation of (6). The cephalosporin oxygenases clearly have a close evolutionary relationship with IPNS (Cooper, 1993) and comparison of their active sites is of interest, particularly with regard to defining the interactions responsible for 2-oxoglutarate binding and turnover.

DAOCS from *S. clavuligerus* was first cloned and over-expressed in *Escherichia coli* as insoluble protein, which was refolded to give soluble, active enzyme for characterization but was unsuitable for crystallization trials (Dotzlaf & Yeh, 1989; Kovacevic *et al.*, 1989). Subsequently, soluble DAOCS was expressed using a plasmid containing the *trc* promoter, but the level of expression and purification methods were not optimal (Morgan *et al.*, 1994). Herein, we report the over-production, efficient purification, crystallization and characterization of DAOCS. The results have implications for the interpretation of the recently reported DAOCS crystal structure (Valegård *et al.*, 1998) and suggest roles for the C termini of DAOCS and related 2-oxoglutarate-dependent dioxygenases.

Results and Discussion

Expression and purification of recombinant DAOCS

High-level expression of the DAOCS gene to produce soluble protein was achieved *via* sub-cloning of the DNA fragment containing the DAOCS gene into the pET11a and pET24a vectors. The resultant plasmids (pML1 and pHL1, respectively) were transformed into *E. coli* BL21 (DE3). In both cases expression at >25 % of the soluble cell protein was observed two to three hours after induction by IPTG when grown at 27 for 30°C. This level of expression was ca ten times better than that previously obtained using *E. coli* NM554/pNM88

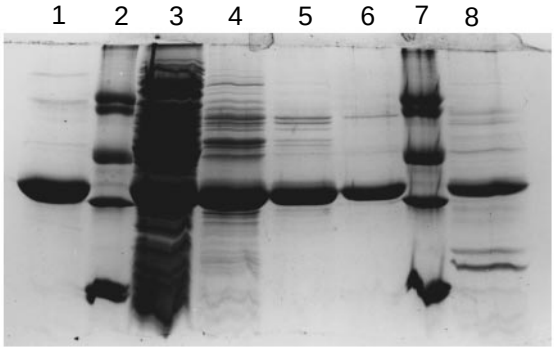

Figure 2. SDS-PAGE analysis of wild-type DAOCS purified by ion-exchange, hydrophobic interaction and gel filtration chromatographies: 1, DAOCS standard (15 μg); 2, markers (9 μg); 3, crude extract (125 μg); 4, Q-Sepharose® HP fractions (34 μg); 5, hydrophobic interaction fractions (26 μg); 6, S-75 fractions (10 μg); 7, markers (9 μg); 8, DAOCS purified from *E. coli* NM554/pNM88(10 μg) (Morgan *et al.*, 1994). Markers (BDH, 10 μg of each protein) were: ovotransferrin (76 and 78 kDa); BSA (66 kDa); ovalbumin (42.7 kDa); carbonic anhydrase (30 kDa); myoglobin (17.2 kDa); cytochrome c (12.3 kDa).

(Morgan *et al.*, 1994) as judged by SDS-PAGE. Soluble expression was not observed when cells were grown at 37 °C. The pET24a vector was preferred since it allows the use of single-stranded mutagenesis techniques. Unlike the pET11a vector, the pET24a vector uses kanamycin rather than ampicillin (i.e. β-lactamase mediated) resistance as the selection method and although we could not find any evidence for contamination of purified DAOCS by β-lactamase, the use of this vector reduces this possibility.

In the optimised method, crude extracts were purified using anion-exchange, hydrophobic interaction and gel filtration chromatographies (Figure 2). The use of SOURCE® 15ISO resin enabled very rapid (less than 30 minutes) concentration and purification of the pool from a Q-Sepharose® HP column. It was possible to purify 150-200 mg of active, crystallography-grade DAOCS within 24 hours (Table 1).

Electrospray ionisation mass spectrometry (ESI MS) of DAOCS gave a mass of 34,554 (±3) Da in agreement with the calculated value (34,551 Da; Figure 3(a)). The predicted N-terminal amino acid sequence (including the N-terminal methionine) was obtained for the first 15 residues (data not shown). The UV-visible spectrum of wild-type apo-DAOCS showed a absorbance maximum at 278 nm ($\varepsilon = 33$, 578 M^{-1} cm^{-1}), with no significant absorbance above 300 nm. DTNB titrations (Habeeb, 1974) in the presence/absence of SDS were consistent with the presence of seven cysteine residues as predicted. In the absence of SDS, four of the cysteine residues were derivatized significantly faster than the other three. Examination of the DAOCS structure (Valegård *et al.*, 1998; K. Harlos & M. D. Lloyd, unpublished results) suggests that all of the cysteine residues are relatively exposed to solvent but it was not possible to correlate specific residues with the observed DTNB titration data.

As noted previously (Sami *et al.*, 1997; Zhang *et al.*, 1997) the errors in apparent K_m and k_{cat} values determined from preliminary steady-state kinetic analysis for Fe(II)-dependent oxidizing enzymes may well be significant and caution should be exercised in drawing mechanistic conclusions from relatively small (i.e. less than an order of magnitude) differences. Purified DAOCS had the following apparent kinetic parameters for penicillin N (**1**): $K_m = 6.6$ (±0.8) μM and $k_{cat} = 0.42$ (±0.05) s^{-1} (specific activity = 727 (±86) nmol min per mg). Adipoyl-6-APA (**8**) has been previously shown to be a (poor) substrate for the enzyme (Shibata *et al.*, 1996), being converted into adipoyl-7-ADCA (**9**) with an apparent $K_m = 1.30$ (±0.10) mM and $k_{cat} = 0.073$ (±0.0003) s^{-1} (127 (±5.3) nmol/min per mg; Figure 4). Penicillin G (**10**) was also converted to the corresponding cephem (**11**) with the following apparent kinetic parameters: $K_m = 2.03$ (±0.12) mM; $k_{cat} = 0.062$ (±0.003) s^{-1} (specific activity = 108 (±5.2) nmol/min per mg). These are similar to the previously reported values ($K_m = 1$ mM; $V_{max} = 87$ nmol/min per mg; Morgan, 1994). In preparative conversions using a higher enzyme: substrate ratio, ca 20-30 % conversion of penicillin G (**10**) to cephem (**11**) was observed. Analogous preparative experiments with penicillin N (**1**) demonstrated >95 % conversion to DAOC (**2**).

Based on the present analyses the differences in k_{cat} for the three substrates analysed are probably insignificant. The differences in the apparent K_m values for penicillin N (**1**) compared to penicillin G (**10**) and adipoyl-6-APA (Shibata *et al.*, 1996) are greater being ca 100-fold. Interpretation of these apparent K_m values as indicators of binding ability for different substrates to DAOCS should be regarded as tentative, but the available data, implying that penicillin G (**10**) and adipoyl-6-APA (**8**) bind to DAOCS with similar affinities, suggest

Table 1. Purification of DAOCS from *E. coli* BL21 (DE3)/pML1

Purification step	Protein (mg/ml)	Total protein (mg)	IU/mg	Total IU
Crude extract	5.70	1727	N/D	N/D
Q-Sepharose® HP (13-22)	1.60	400	42	16,800
SOURCE® 151SO (3-7)	2.08	208	39	8112
Superdex® 75 (18-32, 49-62)	1.11	169	66	11,154

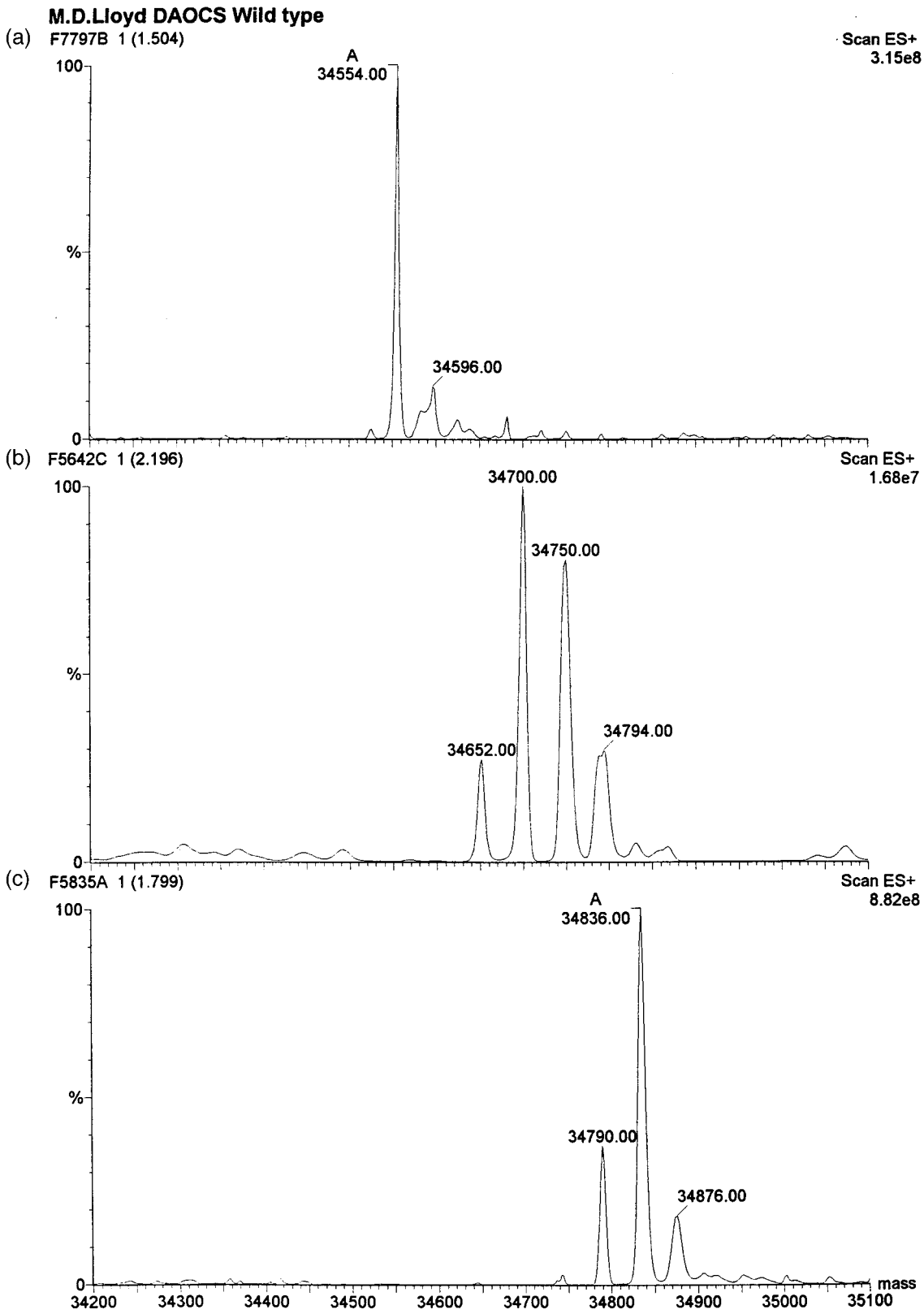

Figure 3. (a) ESI MS of recombinant wild-type DAOCS (top); (b) ESI MS of the recombinant selenomethionyl-DAOCS (grown with 25 μg/ml SeMet) (centre); (c). ESI MS of the recombinant selenomethionyl-DAOCS (grown with 50 μg/ml SeMet) (below). Note the presence of a heavier species at 34,875 (±2.3) Da. The mass difference (ca 40 Da) is inconsistent with the incorporation of an additional selenium atom (ca 47 Da) or oxidation (32 or 48 Da for two or three additional oxygen atoms). It is possible that this species represents an alternative modification(s) or a contaminant.

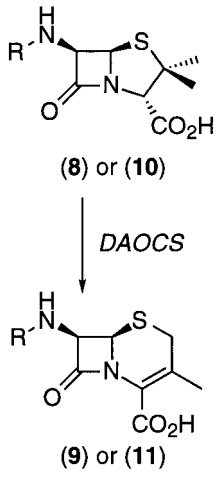

Figure 4. Conversion of adipoyl-6-APA (**8**) to adipoyl-7-ADCA (**9**), and penicillin G (**10**) to phenylacetyl-7-ADCA (**11**) by DAOCS.

that the amino group plays an important role in the binding of the α-aminoadipoyl-side-chain of penicillin N (**1**).

IPNS has a very lax substrate selectivity and is able to catalyse the cyclisation of many analogues of ACV (**6**) (Baldwin & Bradley, 1990), including the relatively efficient conversion of adipoyl-L-cysteinyl-D-valine to adipoyl-6-APA (**8**) and D-(α-aminoadipoyl)-L-cysteinyl-D-valine to penicillin N (**1**) (Baldwin *et al.*, 1984, 1990). In contrast DAOCS apparently has tighter selectivity, at least with respect to the presence of the amino group in the side-chain of its substrates. This may be related to the evolution of the pathway and the fact that penicillin N (**1**) but not isopenicillin N (**7**) is a substrate for DAOCS and DAOC/DACS.

Various metals, including cadmium, cobalt, chromium, copper and manganese salts were screened for their ability to catalyse the conversion of penicillin N (**1**) to DAOC (**2**) and as inhibitors of the reaction (data not shown). Catalysis was only observed in the presence of added Fe^{2+} or Fe^{3+} (the latter has ca 34 % relative specific activity to the former under standard incubation conditions), with the activity observed in the latter case presumably resulting from reduction in solution. When 2 mM Fe(III) was added to the standard incubation mixture containing 2 mM Fe(II) it was inhibitory (>80 % inhibition). $Cd(OAC)_2$ and $CuCl_2$ effected complete inhibition at 2 mM, whilst 2 mM $CoCl_2$ caused ca 50 % inhibition and $NiSO_4$ caused ca 25 % inhibition. The other metal salts tested ($CrK(SO_4)_2$, $MnCl_2$ and $SnCl_2$) showed little or no effect on activity.

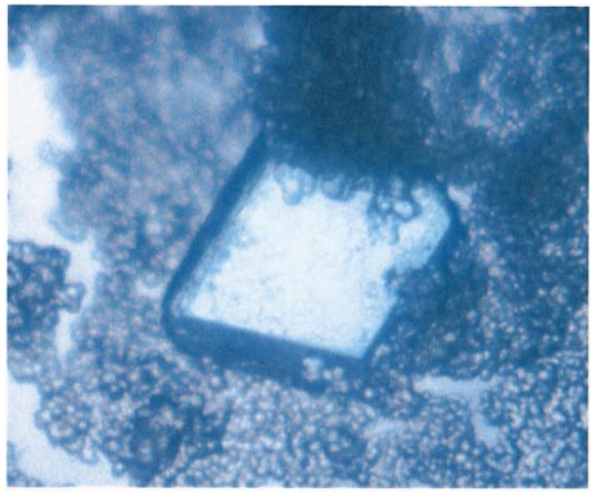

Figure 5. An *R3* crystal of wild-type DAOCS.

Crystallization of DAOCS

The first conditions leading to DAOCS crystals used 100 mM Tris-HCl pH 8.5 buffer containing 2 mM 2-oxoglutarate and ammonium sulphate. These were refined to pH 7.0 and 100 mM Hepes-NaOH buffer containing 5 mM monopotassium 2-oxoglutarate. Crystals with dimensions of 0.2 mm × 0.2 mm × 0.2 mm appeared after three to eight weeks (Figure 5). The space group of the crystal was *R*3 and with a single DAOCS molecule in the asymmetric unit, with the following unit cell dimensions: $a = b = 106.4$ Å, $c = 71.2$ Å; $\alpha = \beta = 90°$, $\gamma = 120°$ (in the hexagonal setting). The predicted density V_M was 2.65 Å^3/Da (Matthews, 1968). All crystals obtained so far were merohedrally twinned with twinning ratios between 0.06 and 0.45 (Terwisscha van Scheltinga *et al.*, unpublished results) and diffracted X-rays beyond 1.3 Å resolution (Valegård *et al.*, 1998).

EXAFS

EXAFS studies were carried out in order to compare the co-ordination chemistry of DAOCS in solution and crystalline states. This is important because studies on IPNS (Roach *et al.*, 1995, 1997) indicate that significant conformational changes affecting the active site and possibly the co-ordination chemistry of iron(II)-dependent oxidizing enzymes occur upon substrate binding. Significant aspects of the mechanism of 2-oxoglutarate-dependent dioxygenases also remain unclear; for example, it is not known if the 2-oxoglutarate is ligated to the iron in a monodentate or bidentate fashion upon binding and reaction of dioxygen, and at what stage carbon dioxide is released from the iron during catalysis.

The Fe K-edge positions for Fe(II) DAOCS alone and in the presence of 2-oxoglutarate of 7121.2 and 7121.4 eV, respectively, are both consistent with the Fe(II) oxidation state (Randall *et al.*, 1993). The

Fe K-edge EXAFS and Fourier transform data (Figure 6(a)) from the Fe(II)-DAOCS complex showed contributions from several shells of backscatterers. The backscattering contributions from the inner shell were successfully simulated using light atoms (C, N, O) only, with no evidence of coordination from heavier elements such as sulphur. Features in the Fourier transform at ca 3 Å and at ca 4.2 Å are characteristic of imidazole groups (Figure 6(a) and (b)). Fits were attempted using 1-3 imidazole groups, including multiple scattering, with other light atoms to complete the inner coordination sphere. The best fit was found with two imidazole groups co-ordinating to the iron with Fe-N of 1.96 Å, three oxygen (or nitrogen) atoms at 2.11 Å, and one other light atom at 2.04 Å. A Fe-N bond distance of 1.96 Å is more consistent with an imidazolate ligand rather than imidazole. These conclusions are consistent with the results obtained from the crystal structure of the DAOCS-Fe(II) complex (Valegård *et al.*, 1998), which show octahedral ligation of the iron by His183, His243, Asp185 and three water molecules (Figure 7(a)).

However, the experimental and simulated EXAFS of the DAOCS-Fe(II) complex were not in complete agreement, in particular a feature in the Fourier transform at ca 3.3 Å was not readily fitted by the data analysis given above. We attempted to reproduce this feature by including backscattering from a single heavy atom such as iron or by several light atoms. However, reproduction of the magnitude of the peak using light atoms required unrealistically low or negative Debye-Waller factors. The use of a heavier backscatterer gave the correct amplitude in the Fourier transform but the improvement in fit of the EXAFS was insufficient to justify the inclusion of the additional parameters. The best fit was found using a light atom

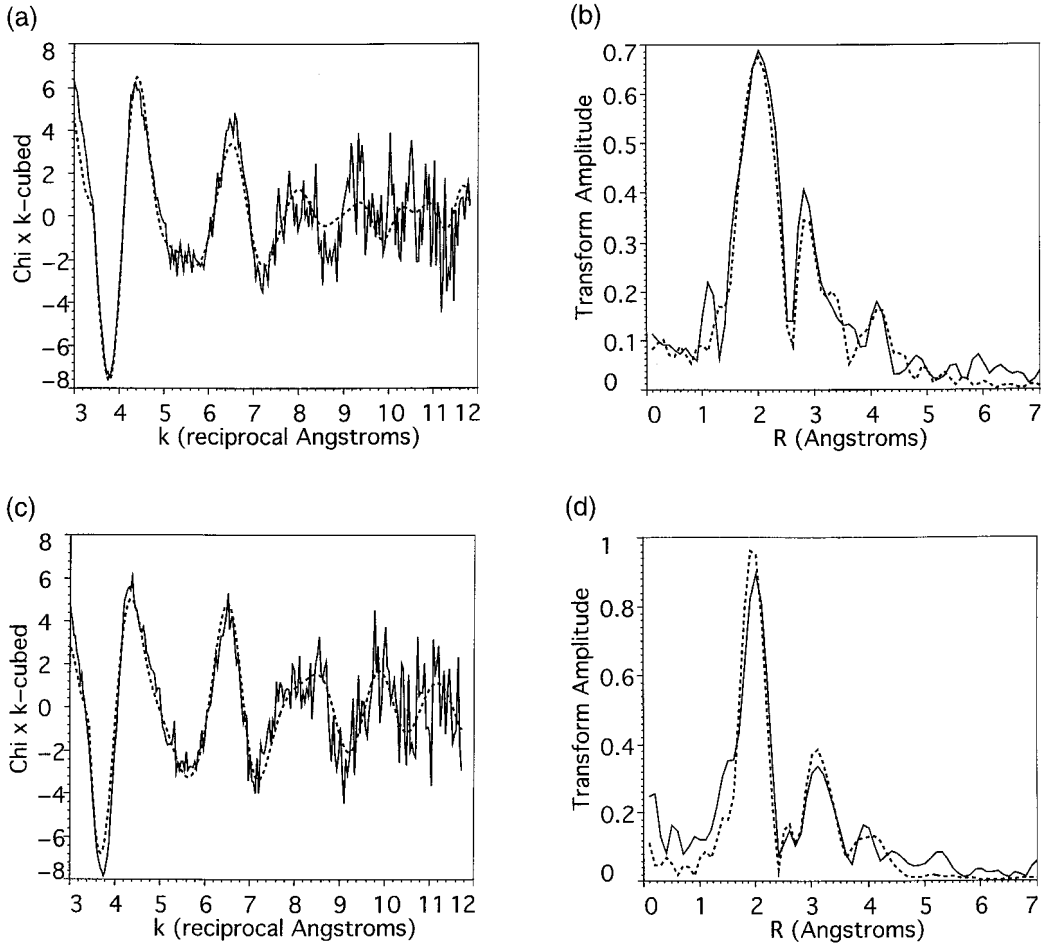

Figure 6. Fe K-edge EXAFS data in 10 M Tris-HCl at ca 80 K and its Fourier transformations (continuous lines) together with the optimum simulation achieved (broken lines). (a) DAOCS-Fe(II) complex (above), optimum simulation: three O atoms at 2.11 Å (Debye-Waller parameter, $2\sigma^2$, 0.008 Å^2); two imidazole groups with Fe-N of 1.96 Å (0.002 Å^2), Fe--C of 2.92 Å (0.004 Å^2), Fe--C/N of 4.16 Å (0.008 Å^2); plus a linear Fe-X-Y group with X atom at 2.04 Å (0.004 Å^2) and Y atom at 3.27 Å (0.005 Å^2). (b) DAOCS-Fe(II)-2-oxoglutarate complex (below), optimum simulation: one atom at 2.08 Å (Debye-Waller parameter, $2\sigma^2$, 0.004 Å^2); two imidazole groups with Fe-N of 1.99 Å (0.001 Å^2), Fe--C of 2.92 Å, (0.004 Å^2), Fe--C/N of 4.10 Å (0.012 Å^2); a 2-oxocarboxylate group with two Fe-O of 2.08 Å (0.002 Å^2), Fe--C of 2.80 Å (0.007 Å^2), Fe--C of 4.41 Å (0.004 Å^2); plus a linear Fe-X-Y group with X at 2.03 Å (0.003 Å^2) and Y atom at 3.33 Å (0.004 Å^2). The estimated uncertainty in the inner shell distances is ±0.03 Å.

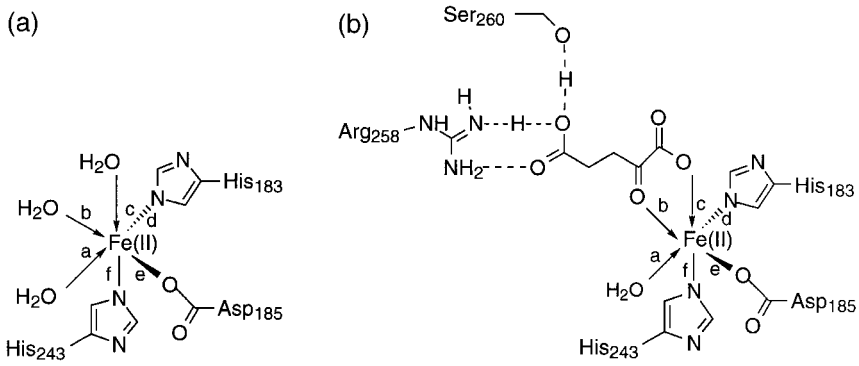

	X-ray (Valegård *et al.*)	EXAFS (This study)	X-ray (Valegård *et al.*)	EXAFS (This study)
a =	2.2 Å	2.04 Å	2.2 Å	2.03 Å
b =	2.1 Å	2.11 Å	2.2 Å	2.08Å
c =	2.1 Å	2.11 Å	2.1 Å	2.08 Å
d =	2.2 Å	1.96 Å	2.1 Å	1.99 Å
e =	2.2 Å	2.11 Å	2.2 Å	2.08 Å
f =	2.2 Å	1.96 Å	2.2 Å	1.99 Å

Figure 7. Co-ordination of the Fe(II) atom in DAOCS (a) without 2-oxoglutarate (left); (b) with 2-oxoglutarate (right). The ligand opposite His183 is shown as a water molecule as in the crystal structures. The EXAFS data, however, suggest the possible presence of an alternative ligand in this position; see the text for details. This species is assigned as being *trans* to His183 since the EXAFS data indicate its presence in both the DAOCS-Fe(II) and DAOCS-Fe(II)-2-oxoglutarate complexes.

(X = O/N/C) at 2.04 Å and another light atom (Y) at 3.27 Å with the inclusion of multiple scattering for a linear Fe-X-Y group (see below).

The EXAFS associated with the Fe K-edge of the DAOCS-Fe(II)-2-oxoglutarate complex and its Fourier transform (Figure 6(b)), whilst similar to the corresponding information for the DAOCS-Fe(II) complex, showed significant differences (notably in the EXAFS between 8 and 10 $Å^{-1}$), indicating that the Fe(II) site has been perturbed by the presence of 2-oxoglutarate. The EXAFS was successfully interpreted by backscattering from two histidine groups (Fe-N at 1.99 Å) with a bidentate *O,O*-co-ordinated 2-oxoglutarate with Fe-O distances of ca 2.08 Å, with another O atom at this distance and a light (O or N) atom at 2.03 Å (Figure 6(b)). As for the DAOCS-Fe(II) complex, a successful interpretation of the Fe K-edge EXAFS and its Fourier transform required inclusion of backscattering from a linear Fe-X-Y arrangement with the light atoms X and Y being 2.03 and 3.33 Å from the iron. Thus, the Fe K-edge EXAFS imply the 2-oxoglutarate replaces two water molecules bound to the iron in the Fe(II) DAOCS complex, which is entirely consistent with the crystal structure of the same complex (Valegård *et al.*, 1998) which shows bidentate binding of 2-oxoglutarate to the iron, *via* the keto-oxygen and one oxygen of the carboxylate group (Figure 7(b)). Since the unusual feature in the EXAFS at ca 3.3 Å is present both before and after 2-oxoglutarate binding the simplest explanation is that it results from a ligand binding to the iron *trans* to His183, the proposed binding site for dioxygen. However, in the crystal structure this ligand is clearly a water molecule. The identity of the Fe-X-Y group proposed on the basis of the EXAFS studies is unknown; an average X-Y distance of ca 1.27 Å is indicative of a bonded contact but the linearity of the arrangement is surprising and appears to preclude X and Y coming from the carboxylate group of Asp185. Contaminants derived from dioxygen (such as superoxide or peroxide) can probably be excluded, since the Fe K-edge position indicates the presence of iron(II) at the active site. The possibility that this feature arises due to ligation of sodium azide (derived from the buffer) by the iron is also unlikely because a non-linear Fe-N bond would be expected. This discrepancy between the crystallographic and frozen solution EXAFS studies will have to be resolved by further experimentation and analysis.

Thus, the EXAFS study provides evidence that the crystal structure reflects solution binding of 2-oxoglutarate (Figure 7(b)). Although a reasonable proposal, care should be taken in assuming that the 2-oxoglutarate remains bound to the iron in a bidentate manner at all times during the catalytic cycle prior to fragmentation of 2-oxoglutarate into carbon dioxide and succinate. It is possible that binding of dioxygen and/or substrate triggers a rearrangement to monodentate binding. Spectroscopic studies on 2,4-(dichlorophenoxy)acetate/2-oxoglutarate dioxygenase complexed to Cu(II) (substituting for Fe(II)) and 2-oxoglutarate indicate monodentate binding of 2-oxoglutarate and the carboxylate of the substrate (Whiting *et al.*, 1997). However, it is likely that the substitution of Cu(II) for Fe(II) significantly perturbs the co-ordination chemistry and more recent spectroscopic studies on complexes formed between clavaminate synthase, iron and 2-oxoglutarate indicate bidentate binding of the latter (Pavel *et al.*, 1998).

The largest discrepancies between the bond lengths obtained from X-ray crystallographic and EXAFS measurements are for the iron(II)-histidinyl residue bonds. Bond lengths obtained by X-ray crystallography suggest imidazole ligands, whilst the EXAFS measurements are more consistent with imidazolate ligands. These differences may be partially a consequence of the different buffer conditions used in these studies, Hepes-NaOH (pH 7.0) with ammonium sulphate in the former case and 50 mM Tris-HCl (pH 7.5), 0.3 mM NaN_3 in the latter. However, in general the atomic distances between a metal and lighter ligands are usually over-estimated in refined X-ray structures of proteins. An analysis of available data demonstrates these distances are systematically longer than those obtained from EXAFS measurements. This suggests that the differences arise from technical procedures rather than inherent structural differences between crystalline and solution states. There may be a number of reasons for the apparent discrepancies. During refinement, in some cases, the iron-ligand distances are treated as non-bonded atoms without additional restraints. Under these conditions, non-bonded contact parameters dominate the refinement, which results in increased bond lengths. This mistake can be corrected for, e.g. by removing such restraints around the metal and its immediate environment, and fixing the distances in subsequent restrained refinement to the values obtained. This procedure often produces bond lengths which agree more closely with values obtained from EXAFS measurements. However, there is another factor to be considered. At the usual resolutions of protein structures (1.5-3.0 Å), series termination errors in Fourier synthesis can produce sizeable ripples around heavy metal scatterers, pushing apparent electron densities from lighter ligands to somewhat longer distances than they may be in reality. The number, depth and location of such ripples depends on the resolution and completeness of the data set. At very high resolutions (such as those in small molecule structures) these ripples become negligible. However, at the resolutions of most protein structures they will be present and systematically produce slightly longer distances than EXAFS measurements, even without the restraints in the X-ray refinement. A source of error in EXAFS measurements should also be considered in situations such as those described herein, where the inner co-ordination sphere of the metal involves atoms with very similar backscattering characteristics at similar but not identical distances. In the interpretation of the EXAFS it is difficult to unambiguously determine the individual contributions to the overall backscattering. Useful clarification can be obtained when outer shells provide multiple scattering contributions, e.g. those observed with imidazole groups.

Role of methionine-180

The DAOCS crystal structures (Valegård *et al.*, 1998; K. Harlos & M.D. Lloyd, unpublished results) reveal that all (but one) methionine residues are located relatively close to the surface of the protein. The exception, methionine-180, is located within the active site and its side-chain becomes ordered upon binding of 2-oxoglutarate and/or iron(II). In the DAOCS-Fe(II)-2-oxoglutarate complex Met180 is in van der Waals contact with the C-2 atom of the 2-oxoglutarate (Valegård *et al.*, 1998; K. Harlos & M. D. Lloyd, unpublished results). The presence of an easily oxidizable side-chain so close to the reactive centre of DAOCS is somewhat surprising and it is probable that its oxidation to a sulphoxide or sulphone would affect the binding of 2-oxoglutarate and hence catalysis. Despite the observations that selenomethionine residues are more easily oxidized than methionine residues and crystallization of the selenomethionine derivative required anaerobic conditions, there were no apparent functional differences between the wild-type and selenomethionine derivative (Materials and Methods, Figure 3), nor was there any clear ESI MS evidence for oxidative modifications of the derivative. Similar specific activities were obtained for both, suggesting that the oxidative chemistry occurring within the DAOCS active site is tightly controlled and directed away from Met180, making the possibility of a methionine sulphoxide or radical intermediate during catalysis unlikely.

Significance of the trimeric nature of DAOCS

The solution of the DAOCS structure (Valegård *et al.*, 1998; K. Harlos & M. D. Lloyd, unpublished results) demonstrates that it crystallizes as a trimer with one molecule in the asymmetric unit (Figure 8). The C-terminal residues from one DAOCS molecule project towards the active site of an adjacent sub-unit in a cyclic manner, forming a trimer. The key intermolecular interactions resulting from trimerization are shown in Table 2. Gel filtration analysis indicated that in solution apo-DAOCS exists as an equilibrium mixture of monomeric (est. 28.9 kDa) and trimeric (est. 92.9 kDa) forms. The presence of 5 mM 2-oxoglutarate had no apparent effect on the equilibrium position. Dynamic laser light scattering studies showed that apo-DAOCS is predominately trimeric at 15-20 °C, pH 7.0. At 20 °C the mean hydrodynamic radius was 4.2 nm, corresponding to an apparent mass of 96 kDa. The protein showed a bimodal size distribution in which the trimeric and monomeric forms are in equilibrium. This equilibrium was temperature-sensitive, and shifted towards the monomeric form at 15 °C (mean radius = 3.4 nm, 57 kDa). Addition of 10-100 mM 2-oxoglutarate alone did not effect the equilibrium position. Addition of 5-10 mM $FeSO_4$ alone to DAOCS induced a shift towards the monomeric form of the enzyme (mean

hydrodynamic radius 3.2 nm, 48 kDa at 20 °C). Addition of 5-10 mM $FeSO_4$ with 25-50 mM 2-oxoglutarate resulted in almost complete dissociation to the monomeric form at 20-37 °C (mean radius 2.9 nm, 39 kDa). These studies imply that it is the monomeric form of DAOCS which is catalytically active. Indirect support for this proposal came from X-ray crystallographic results (Valegård *et al.*, 1998), which show a clear movement of the C terminus upon binding of iron(II), which was predicted to cause dissociation into the monomer. Further oligomerisation *via* active site and C-terminal tail interactions may be partially responsible for the observation that DAOCS forms inclusion bodies when over-produced, particularly at 37 °C. During refolding studies (data not shown) on DAOC/DACS an apparent temperature-dependent tendency to form oligomers was also noticed and this may also reflect the operation of an oligomerization process.

Role of the C terminus and substrate binding

Comparison of the DAOCS and IPNS-Mn structures reveals strikingly similar general relationships between their active sites and C termini. In the structure of IPNS complexed to manganese (substituting for Fe(II)) Gln330 ligates to the metal, and thus the C terminus forms a ''lid'' over the active site, an arrangement also observed in the case of DAOCS. However, in the case of the DAOCS crystal structure the C-terminal lid is derived not from the same molecule, but from a neighbour in the trimeric unit. The active sites of DAOCS and IPNS are unusual in that they are located within, rather than external to, the jelly roll barrel which forms the core of their structures. It is possible the presence of a C-terminal lid (which combined with other conformational changes would constitute a closed form of the enzyme) on the active site (in either monomeric or trimeric forms) stabilizes the jelly role core of the resting enzyme, thereby reducing the possibility of unfolding and subsequent oxidative or proteolytic damage. Formation of the oligomers *in vivo* may also be significant if high concentrations of enzyme are present such as in an antibiotic production strain. The potential of the C terminus to adopt different conformations and its involvement in oligomerization should also be noted in respect of crystallization experiments on enzymes of the DAOCS family, in particular with regard to choice of mutant or isoenzyme for study.

Both IPNS and DAOCS are unstable *in vitro*, particularly under catalytic conditions. In part inactivation results from oxidative damage resulting from reactive oxidizing species (e.g. hydrogen peroxide) generated from the requisite cofactors (iron, ascorbate, dioxygen). ACCO is particularly sensitive to this type of oxidative damage, undergoing extensive fragmentation (Barlow *et al.*, 1997). However, it is clear that oxidative damage to a single form of the enzyme is not the only mode of inactivation and it is also unlikely that oxidation (which is likely to be significantly irreversible) explains the differences between the *in vitro* and *in vivo* inactivation rates. Upon standing in buffer recombinant ACCO from tomato fruit undergoes a confor-

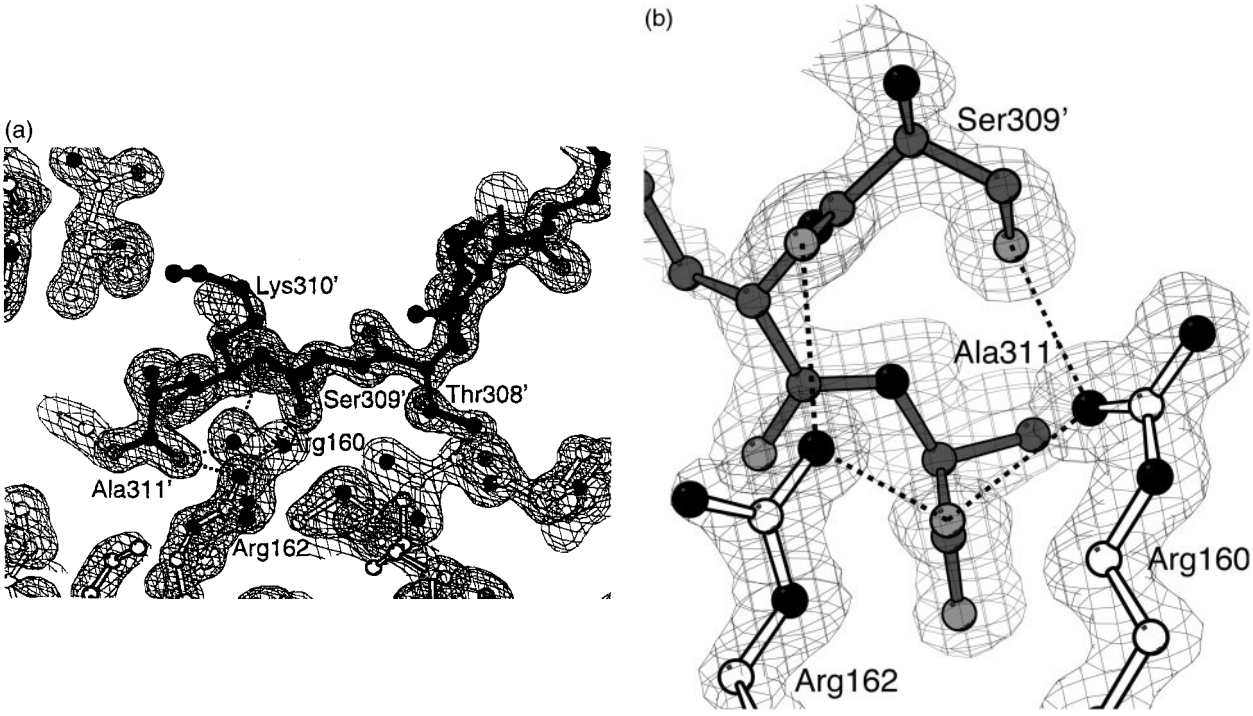

Figure 8. (a) Close up view of the C-terminal arm interactions with the neighbouring sub-unit. (b) Close up view of #Ala311 and its interactions with Arg160 and Arg162. View is perpendicular to that in (a).

Table 2. Intermolecular hydrogen bonding interactions in *R*3 DAOCS crystals

Atom 1	Atom 2	Distance (Å)
O Pro69	N Ala240	2.9
$O^{\gamma 1}$Thr72	O Gly282	2.6
O Gly79	$N^{\eta 1}$Arg242	3.0
O Gly79	$N^{\eta 2}$ Arg242	3.0
N^{ε} Arg125	$O^{\delta 2}$ Asp214	3.0
$N^{\eta 1}$ Arg160	O^{γ} Ser309	2.9
$N^{\eta 1}$ Arg160	OT2 Ala311	2.8
$N^{\eta 2}$ Arg162	O Ser309	2.9
$N^{\eta 2}$ Arg162	OT2 Ala311	2.7
$N^{\eta 1}$ Arg266	$O^{\delta 2}$ Asp284	2.9
N Ser286	O Gly300	2.9
O^{γ} Ser286	O-Gly299	2.8
$N^{\varepsilon 1}$ Trp297	$O^{\delta 1}$ Asn301	2.9

mational change to a less active form in which the main secondary structure elements are conserved. Supporting evidence for the proposal that a conformational change contributes to inactivation includes mutagenesis experiments which demonstrate that oxidative fragmentation of ACCO, which occurs as a burst upon addition of substrates/cofactors, only occurs in a form of the enzyme in which the iron is ''incorrectly'' ligated for catalysis (Zhang *et al*., 1997).

The predicted inherent mobility in the C-terminal region of DAOCS and related enzymes, specifically the interconversion between open and closed forms, and the possibility of misfolding (and enhanced susceptibility to oxidative damage) in the former or intermediate forms, may well be a major cause of the notorious instability of this family of enzymes. It also explains the discrepancy between the *in vitro* and *in vivo* inactivation rates, since refolding mechanisms will exist in the latter case.

In the IPNS-Mn structure Gln330, the penultimate residue on the C terminus, acts as a fourth protein-based iron ligand (Roach *et al*., 1995), which is displaced upon ACV (**6**) binding (Roach *et al*., 1997). In contrast, the DAOCS structure reveals only three protein-derived iron ligands and the EXAFS data do not provide evidence for a fourth protein ligand. Thus, the DAOCS studies support mutagenesis studies with IPNS, concluding that iron ligation by a C-terminal residue is not required for catalysis (Sami *et al*., 1997; Borovok *et al*., 1996). The structures suggest that the DAOCS C terminus may assist in ordering binding of substrates to the active site. Thus, whilst 2-oxoglutarate can co-ordinate to the iron in the closed form, in order for penicillin N (**1**) to bind to the active site of DAOCS, the C terminus must be displaced to give a more open form of the enzyme. Thus, although DAOCS crystallizes as a trimer and can exist in this form in solution, it is the monomer which is the catalytically active form. A possible hinge allowing movement of the C terminus with respect to the active site is between residues 298 and 302 (I**GGNY**), a well conserved sequence in DAOCS (*S. clavuligerus, Norcardia lactamdurans*), DACS (*S. clavuligerus, Norcardia lactamdurans*) and DAOCS/DACS (*C. acremonium*) (Cooper, 1993), suggesting that the C terminus is also important in the DACS and DAOC/DACS catalytic cycles (see below).

Examination of the interactions between the C-terminal residues (Asn304′ to Ala311′) of one DAOCS molecule and the active site of another (Figure 8) suggests a binding mode for the penicillin nucleus (Figure 9(a)). The penam C-3 carboxylate group probably occupies an analogous position to that of Ala311′ from a symmetry-related molecule in the active site (Figure 8), forming electrostatic interactions with Arg162 and Arg160 (Figure 9 and Table 2). The side-chain of Arg160 may also be in position to form a hydrogen bonding interaction with the β-lactam nitrogen/carbonyl. Asn304, close to the C terminus of the enzyme, may form a hydrogen bond with the amide bond linking the side-chain to the penicillin nucleus.

Although anticipated from sequence analyses, the observation that the side-chains of the highly conserved Arg258 and Ser260 residues bind to the 5-carboxylate of 2-oxoglutarate is of interest, since the analogous residues in IPNS (together with Tyr189 and a water molecule) bind the ACV (**6**) valine carboxylate. Within the family of known iron-dependent oxidizing enzymes clearly related by sequence to DAOCS only two, IPNS and ACCO, do not use a 2-oxoglutarate cosubstrate with ACCO apparently using ascorbate in the place of 2-oxoglutarate. Thus, it seems most probable that IPNS evolved from a 2-oxoglutarate-dependent oxygenase rather than *vice versa.*

The presence of Arg160 and Arg162 in the DAOCS active site is a significant difference compared to that of IPNS (Figure 9(b)). In the structure of IPNS complexed to iron(II) and ACV (**6**), apart from the residues complexing to the iron and those forming electrostatic interactions with the valine carboxylate, the active site is largely devoid of polar residues. In the proposed mechanism for IPNS (Roach *et al*., 1997) the iron-bound oxidizing species are isolated from the environment in part by the presence of the ACV (**6**) substrate, which is wrapped around them. The presence of the extra electrostatic interactions in the DAOCS active site relative to that of IPNS reflect its requirement to bind and position an extra substrate with a carboxylate group, penicillin N (**1**).

Mechanistic implications

Kinetic studies on other 2-oxoglutarate-dependent oxygenases (Holme, 1975) have demonstrated ordered sequential binding of 2-oxoglutarate and the prime substrate followed by that of dioxygen, as shown for DAOCS in Figure 10. Binding of penicillin N (**1**) (and 2-oxoglutarate) probably occurs to an open form of the enzyme. Binding of penicillin N (**1**) may also assist dioxygen binding *via* displacement of the water molecule ligated to

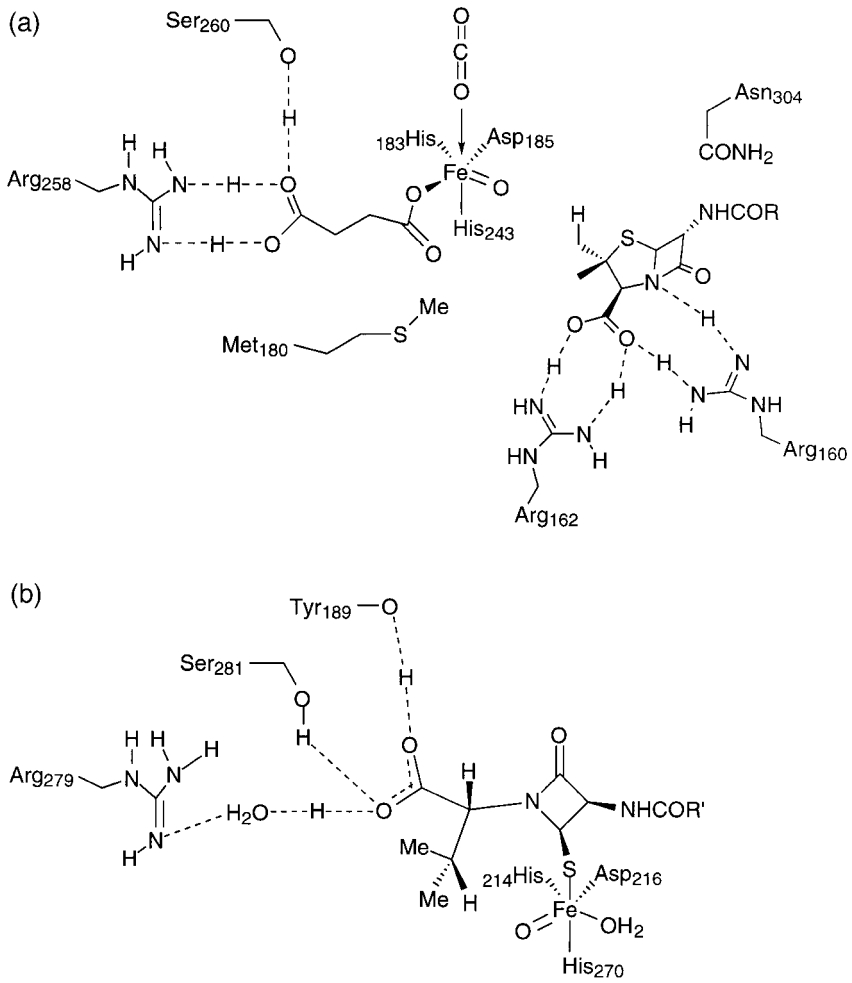

Figure 9. (a) Proposed binding site for the penicillin N (**1**) in the active site of DAOCS, showing the proximity of the reactive ferryl species and the β-methyl group of the substrate. The side-chain of Arg160 may also bind to the β-lactam oxygen. R=D-α-aminoadipoyl. Note the presence of the Met180 side-chain, which is prevented from approaching the iron by the presence of the penicillin. (b) Possible structure for the ferryl/monocyclic β-lactam intermediate in IPNS catalysis as proposed by Roach *et al.* (1997, 1995) on the basis of the structures of the IPNS-Fe(II)-ACV and IPNS-Fe (II)-ACV-NO complexes. ACV=L-δ-α-aminoadipoyl)-L-cysteinyl-D-valine (**6**). R=L-α-aminoadipoyl. Note in the intermediate the C^{α}-C^{β} bond of the isopropyl group of the valine is rotated relative to the tripeptide structures where the C^{β}-H bond, which must be cleaved, projects away from the iron centre.

the iron *trans* to His183. Formation of a ferryl complex may then occur as proposed previously (Valegård *et al.*, 1998) *via* superoxide or peroxide intermediates in an isolated environment, i.e. a closed form of the enzyme. Carbon dioxide may remain co-ordinated to the ferryl iron, possibly as a bicarbonate ion after reaction with water. Together with the carboxylate derived from the succinate continued ligation of the carbon dioxide/bicarbonate may serve to modulate or direct the reactivity of the ferryl species.

Isotopic labelling experiments have demonstrated that cleavage of a C-H bond of the penicillin *pro*-S methyl group occurs before cleavage of the C-3 C-H bond (Baldwin *et al.*, 1991): Binding of penicillin N (**1**) in the proposed manner projects this methyl group directly towards the iron centre whilst the C-3 C-H bond is further away. The isolated nature of the active site in the closed form, the distance of the thiazolidine sulphur from the iron and the requirement for (at least) one of the iron ligands to be decomplexed renders mechanisms involving complexing of the penam sulphur to the iron unlikely. We presently favour a mechanism in which a ferryl intermediate, generated as previously proposed (Valegård *et al.*, 1998), reacts with the *pro*-S methyl group to generate a primary radical (Pang *et al.*, 1984; Townsend *et al.*, 1985). Biomimetic studies (Baldwin *et al.*, 1988) suggest that this species enters an equilibrating manifold of radicals in which a tertiary cepham radical predominates. This may react with the Fe-OH species, either to give DAOC (**2**) and water (Figure 10, path A) or to form the 3β-hydroxymethylcepham (**12**) (Figure 10, path B; Baldwin *et al.*, 1991).

Alternatively, single electron transfer from the intermediate radical(s) may occur (Figure 10, path C) to give a cation, which must lose a proton to give DAOC (**2**) (Figure 10, path D) or which reacts with water/hydroxide to give (**12**) (Figure 10, path E). Since no protein derived functionality, including the side-chains of both Arg162 and Arg160 which are on the ''wrong'' face of the intermediates, is in position to act as a general base to deprotonate the C-2 C-H, it seems likely that (if a cationic mechanism is in operation) one of the three substrate-derived iron ligands acts in this manner. The binding model implies the position *trans* to His183 as the likely location for an iron ligated base. Further, use of a succinate oxygen as a general base would seem unlikely, since it is locked into a highly electron-deficient iron centre. It is possible that the CO_2 derived from 2-oxoglutarate reacts with water to form bicarbonate, which

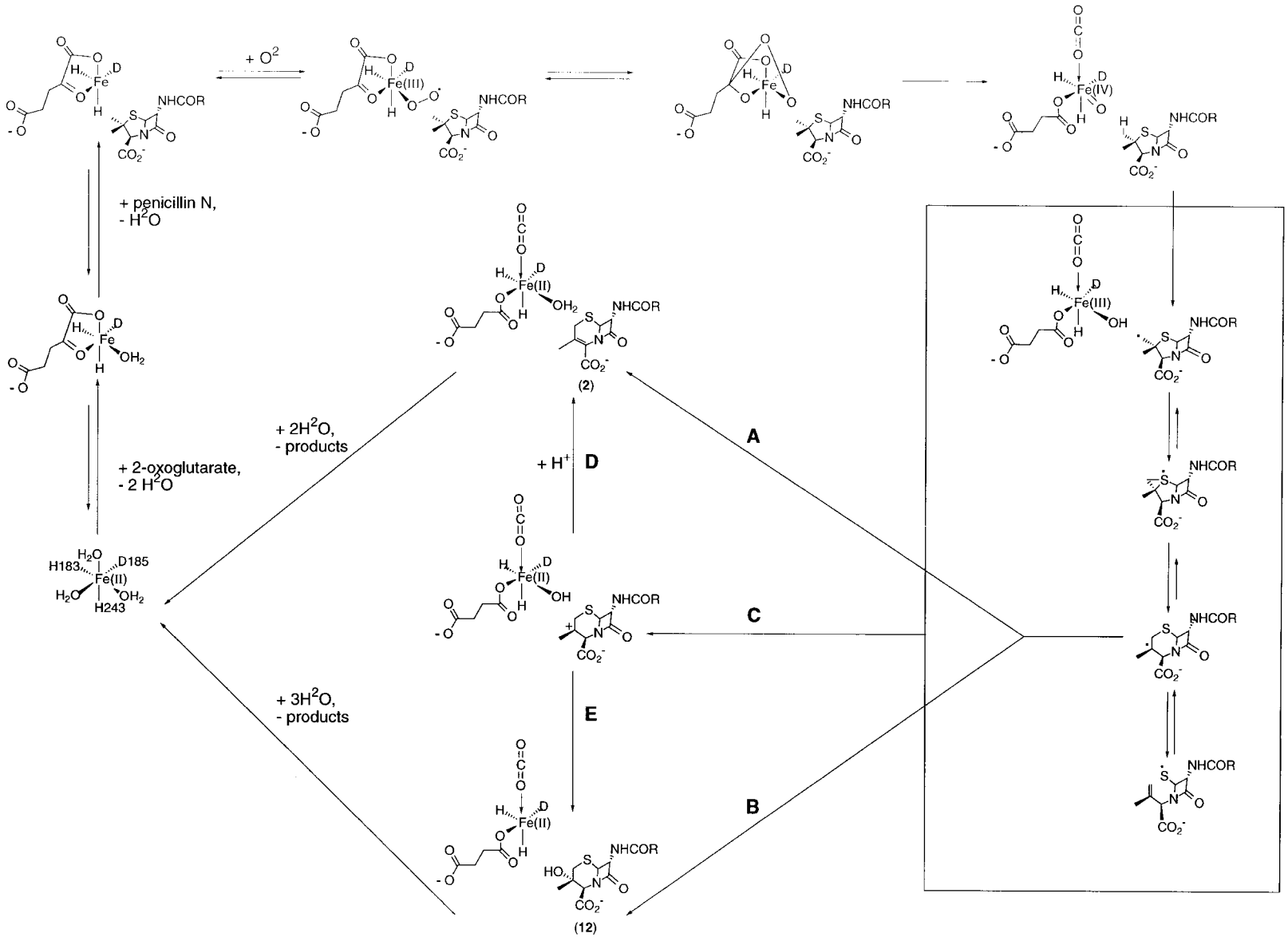

Figure 10. Mechanism for the expansion of penicillins by DAOCS to cephalosporins. The binding of substrate and release of products is probably accompanied by significant conformational changes between ''open'' and ''closed'' forms of the active site (see the text). R=D-δ-(α-aminoadipoyl)-.

acts as a base. In our mechanism this would place the bicarbonate *trans* to His243, possibly rendering it too far away to cleave the C-3 C-H bond directly. Thus, the bicarbonate may serve to increase the basicity of the hydroxyl *trans* to His183, which may act as a base, deprotonating the cationic intermediate to give (**2**) or quench it to give (**12**). Migration of the CO_2 to the hydroxyl group *trans* to His183 is another, less likely, possibility.

Kinetic studies imply that carbon dioxide is the first released product in 2-oxoglutarate-dependent dioxygenase catalysis (Holme, 1975) and it may be that return of the metal to the iron (II) oxidation state facilitates release of CO_2 (or bicarbonate) from the metal, which in turn triggers conformational changes, including movement of the C-terminal region, to give a more open form of the enzyme, allowing release of DAOC and succinate.

DAOCS like other 2-oxoglutarate-dependent oxygenases can catalyse the ''uncoupled'' turnover of 2-oxoglutarate to succinate and carbon dioxide, albeit at a much reduced rate, in the absence of the prime substrate (Myllyharju & Kivirikko, 1997). The uncoupled turnover process has been studied in detail in the case of prolyl-4-hydroxylase, where in the absence of collagen substrate the turnover of 2-oxoglutarate is apparently stoichiometric with that of ascorbate in the presence of excess of the latter (Myllyharju & Kivirikko, 1997). Some substrate analogues can stimulate the uncoupled turnover process without themselves being oxidized and certain mutations can significantly alter the ratio of coupled : uncoupled turnover (Myllyharju & Kivirikko, 1997). The uncoupled turnover process may represent an editing process contributing to the attainment of both substrate and product (with respect to the type of oxidation reaction catalysed) selectivity by the 2-oxoglutarate-dependent enzymes. Conformational flexibility between (partially) open and closed enzyme forms may hinder binding and reaction of dioxygen to an enzyme-Fe(II)-2-oxoglutarate complex to which either the wrong ''prime'' substrate is bound or to one in which the correct prime substrate is incorrectly bound. Furthermore, such flexibility may also allow release of an undesirable or incorrectly bound prime substrate after formation of the ferryl species, which may be reduced back to the iron (II) oxidation state by a relatively non-specific reductant, e.g. ascorbate in the case of prolyl-4-hydroxylase†. The need for such an editing process may be particularly important in the case of prolyl-4-hydroxylase, where the natural substrate is a polymer, collagen, with a considerable degree of secondary structure, which may make precise arrangement of the proline residues within the active sight of prolyl-4-hydroxylase awkward.

The mechanistic complexity of the 2-oxoglutarate-dependent dioxygenases ensures that many questions remain unanswered, but the present work, together with that of the recently reported crystal structures (Valegård *et al*., 1998), places previous mechanistic studies within a structural context and provides new detailed proposals. It is important that future studies are now directed towards the structural characterization of intermediates in the catalytic cycle.

† The release of substrate after formation of the ferryl species offers a plausible explanation for kinetic studies measuring V_{max}/K_m isotope effects using deuterium labelled penicillin Ns (Baldwin *et al*., 1987a). These were interpreted previously as indicating a mechanism involving reversible binding of penicillin N (**1**) to a ferryl intermediate formed by reaction of Fe(II) and 2-oxoglutarate with dioxygen. Note also that the possibility of more than one kinetic mechanism cannot be excluded.

Materials and Methods

Materials

All chemicals were supplied by the Sigma-Aldrich Chemical Co., unless otherwise stated, and were of analytical grade or higher. Penicillin N (**1**) was synthesized by an extension of the reported method (Baldwin *et al*., 1987b). Chromatography systems and columns were obtained from Amersham Pharmacia Biotech. Protein purification was performed on ÄKTA explorer®, FPLC® or BioPilot System. Q-Sepharose® HP (254 ml) was packed into a 60/100 column (I.D. = 6 cm × 9 cm). DEAE Sepharose® FF (30 ml) was packed into aXK16 column (I.D. = 1.6 cm × 15 cm) or 250 ml into a XK50 column (I.D. = 5.0 cm × 12.7 cm). SOURCE® 151SO (33 ml) was packed into a FineLINE® Pilot 35 column. Superdex® 75 was packed into an G32 × 1000 column (Amicon, I.D. = 3.2 cm × 89 cm, 716 ml and a XK26 column (I.D. = 2.6 cm × 60 cm, 320 ml). The following prepacked columns were used: RESOURCE® ISO (1 ml); RESOURCE® Q (6 ml); Mono Q® HR 16/10; Superdex® 200 10/30; NAP-5. SDS-PAGE was performed using the Mini-Protean system (Bio-Rad). Gels were stained using Coomassie brilliant blue and Bismark brown (Lloyd, 1996), and were calibrated with the molecular mass marker kit 12,300-78,000 (BDH). ^1H NMR spectra were obtained in ^2H_2O and referenced to TSP. The anaerobic glove box was supplied by Belle Technology and was supplied with an atmosphere of oxygen-free nitrogen.

Construction of expression vectors

Expression vector pML1 was constructed according to standard protocols (Sambrook *et al*., 1989). Sub-cloning of the fragment of DNA containing the DAOCS gene was performed by digestion of pNM88 (Morgan *et al*., 1994) and pET 11a vectors using *Bam*HI and *Nde*I. The appropriate fragments were isolated by agarose gel electrophoresis, ligated, transformed into *Epicurian coli* XL1 Blue (Stratagene) and plated onto LB-agar containing 100 mg/ml ampicillin. Individual colonies were screened by agarose gel electrophoresis following initial digestion with *Bam*HI/*Nde*I. The required clones were repurified using the Wizard Mini-prep method (Promega), transformed by heat-shock into competent *E. coli* BL21 (DE3) and plated as before. Single colonies were screened for expression in 2TY containing 50 μg/ml ampicillin at 27, 30, and 37°C. The DNA encoding the DAOCS gene was sub-cloned from pML1 into the pET24a vector using an analogous procedure with kanamycin sulphate

(50 μg/ml) as the selection antibiotic. This vector was designated pHL1.

Fermentation of *E. coli* BL21 (DE3)/pML1

E. coli BL21 (DE3)/pML1 was inoculated from a glycerol freeze into 4 × 100 ml of 2TY supplemented with 50 μg/ml ampicillin and grown overnight at 33 °C. The starter culture was used to inoculate 30 l of the same medium supplemented with 5 ml of polypropylene glycol 2025 in a New Brunswick Scientific MPP40 fermenter. The culture was grown at 30 °C, 300 r.p.m. and 30 l/min air for four hours ($A_{600\ nm} = 2.96$). IPTG (0.4 mM, Melford) was added and the culture was grown for a further three hours under the same conditions. Cells were concentrated to ca three litres using a tangential flow concentrator (Satorius) and centrifuged (JA-10 rotor, 10 000 r.p.m., 17,500 *g*, 15 minutes) and stored at −80 °C. Cells containing pHL1 were grown under identical conditions using kanamycin sulphate (50 μg/ml) in place of ampicillin.

Production of the selenomethionine derivative required re-optimization of the fermentation and purification conditions. The methionine auxotrophes B834 (DE3) and B834 (LyS) (DE3) (Pappa *et al.*, 1996) containing the pML1 plasmid gave soluble expression of DAOCS in 2TY medium, but soluble expression was not observed in LeMaster medium (by SDS-PAGE) and consequently *E. coli* BL21 (DE3) was used as the host cell. Small-scale incorporation trials showed that lower incorporation occurred for cultures induced at high A_{600}, increasing post-induction growth times and decreasing selenomethionine concentrations (Figure 3). In the optimized procedure a single colony was inoculated into culture medium consisting of LeMaster media (Hendrickson *et al.*, 1990) (5 ml), non-autoclavable LeMaster medium (0.5 ml), ampicillin (50 μg/ml), 1 × Kao and Michayluk vitamin supplement (growth medium) supplemented with 2TY (0.5 ml) and DL-methionine (40 μg/ml) and grown at 37 °C and 250 r.p.m. This culture was used to inoculate growth medium (2 × 100 ml) supplemented with DL-methionine and grown as before. This culture was used to inoculate a ten litre fermenter containing growth medium and 50 μg/ml DL-selenomethionine and was grown at 37 °C to $A_{600} = 0.8$, induced and allowed to grow for a further two hours before harvesting.

Purification of DAOCS

All manipulations were performed on ice or at 4 °C. All fractions were analysed using 12.5 % (w/v) SDS-PAGE, following initial TCA precipitation for those samples containing ammonium sulphate. Cells expressing wild-type DAOCS (*E. coli* BL21 (DE3)/pML1, 70.15 g) were thawed and resuspended in 280 ml of 50 mM Tris-HCl, 1 mM EDTA (pH 7.5), 2 mM DTT, 1 mM benzamidine-HCl, 1 mM PMSF, 1 μM leupeptin (lysis buffer). Lysozyme (155 mg) was added and the solution was stirred for 15 minutes. Complete cell disruption was achieved by sonication using 4 × 20 second burst on power 5 with 60 seconds cooling between each burst (W-380 sonicator, Ultrasonics Inc.). DNA was removed by precipitation with 1 % (w/v) streptomycin sulphate and 0.1 % (w/v) PEI. After 15 minutes stirring the extract was centrifuged (Beckman, JA-14 rotor, 12,000 r.p.m., 22,000 *g*, ten minutes), loaded onto a Q-Sepharose® HP column which had been equilibrated in 50 mM Tris-HCl, 1 mM EDTA, (pH 7.5), 2 mM DTT, 0.2 mM benzamidine-HCl, 0.2 mM PMSF (column buffer) and washed with 1000 ml of the same buffer at 25 % ml/min. Protein was eluted with a 25-75 % 0.3 M NaCl gradient in the same buffer over 600 ml. All fractions (25 ml) were analysed by 12.5 % SDS-PAGE. Fractions 13-22 (150-220 mM NaCl) were pooled and 260 ml of 3.2 M $(NH_4)_2SO_4$ was added slowly with stirring. This pool was loaded onto a SOURCE® 151SO column which had been equilibrated with 1.6 M $(NH_4)_2SO_4$ in column buffer at 40 ml/min. The column was washed with 100 ml of the same buffer and eluted with a 90-50 % gradient using column buffer supplemented with 20 % (v/v) glycerol over 300 ml with 20 ml fractions collected. The inclusion of glycerol in this buffer is essential for efficient elution of purified protein. Fractions 3-7 (1.3-1.1 M $(NH_4)_2SO_4$) were pooled, concentrated in a 50 ml Amicon stirred cell to ca 13 ml and loaded as 2 × 6.5 ml onto a Superdex® 75 column (716 ml) which had been equilibrated in 100 mM Tris-HCl, 1 mM EDTA (pH 7.5), 2 mM DTT, 0.2 mM benzamidine-HCl, 0.2 mM PMSF (gel filtration buffer). The column was eluted with the same buffer at 2 ml/min and fractions (5 ml) were collected between 280 and 440 ml. Fractions 18-32 (370-440 ml and 49-62 (360-430 ml) were pooled, concentrated to ca 9 ml and exchanged into 10 mM Hepes-NaOH (pH 7.0) using Econo-pak columns (Bio-Rad). Protein was concentrated to 50 mg/ml and frozen on dry ice before storage at −80 °C. It was not possible to measure accurately DAOCS activity in crude *E. coli* extracts, due to inference with the holed-plate assay (Baldwin *et al.*, 1987a,b) by the antibiotic activity of streptomycin sulphate. Assay of DAOCS activity in crude extracts, by HPLC was also difficult because of the presence of other materials which absorb at λ = 254 nm.

The molecular mass of native apo-DAOCS was determined by exchanging into gel filtration buffer and loading 0.38 mg (in 100 μl) onto a Superdex® 200 10/30 column which had been equilibrated in the same buffer at 0.5 ml/min. The column was calibrated using the following proteins (0.125 mg unless otherwise stated): β-amylase (200 kDa); ADH (150 kDa); BSA (66 kDa); ovalbumin (42.7 kDa, 0.31 mg); carbonic anhydrase (29 kDa). An identical analysis was also performed using 5 mM monopotassium 2-oxoglutarate in the buffer and sample.

The expression level for the selenomethionyl-DAOCS was ca threefold less than for the wild-type, possibly due to the toxic effects of the selenomethionine and/or the relatively short induction time, and its purification was performed in the presence of 5 mM DTT to avoid oxidative damage (Hendrickson *et al.*, 1990). Two different ion-exchange column chromatographies (DEAE Sepharose® FF and RESOURCE® Q) at different pH values were required in order to improve the final level of purification. Thus, selenomethionyl-DAOCS was purified from 22 g cells using an identical extraction procedure with 5 mM DTT. The extract was loaded onto a DEAE Sepharose® FF column (30 ml) in column buffer at pH 8.5 and eluted with a 30-70 % 0.4 M NaCl gradient over 135 ml with 10 ml fractions. Further purification of fractions 3-5 was achieved using five runs with a RESOURCE® ISO column (1 ml), eluting with a 90-35 % 1.6 M $(NH_4)_2SO_4$ gradient over 12 ml at pH 7.5 with 1 ml fractions. Fractions 2-6 were pooled and concentrated to 6 ml, loaded as 2 × 3 ml onto a Superdex® 75 column (320 ml) and purified as before with 3 ml fractions. Fractions 20-28 and 70-78 were pooled, diluted with one volume of Milli-Q water and loaded onto a RESOURCE® Q column (6 ml) in column buffer at

pH 7.5. The column was eluted with a 25-75% 0.3 M NaCl gradient over 27 ml with 3 ml fractions. Fractions 3-5 were pooled, buffer exchanged and concentrated to 26.4 mg/ml before storage at −80 °C. The derivative was ca 95% (i.e. less than the wild-type) pure by SDS-PAGE analysis and had a similar specific activity to wild-type DAOCS using penicillin N (**1**) as substrate in the holed plate assay (232 nmol/min per mg compared to 208 nmol/min per mg for wild-type DAOCS control).

Synthesis of G-7-ADCA (11)

(**11**) was prepared from 7-ADCA (5.1 mmol, 1.02 g) and phenylacetyl chloride (7.56 mmol, 1 ml) (Chauvette *et al*., 1971) using THF as the organic solvent and NaOH as the base. The product was solvent extracted into ethyl acetate to give a pale yellow solid (475 mg, 26%). HPLC purification (C_4 Hypersil (250 × 4.6 mm), 25 mM NH_4HCO_3 in 5% (v/v) methanol at 2 ml/min, $\lambda = 254$ nm) gave (**11**) (>95% pure by ^{1}H NMR analysis) with a retention volume of 34-42.8 ml: ^{1}H NMR (500 MHz) δ_H 1.9 (3 H, s, CH_3); 3.25 (1 H, d, $J = 7.5$ Hz, H-4); 3.35 (3 H, s, residual MeOH); 3.55 (1 H, d, $J = 7.5$ Hz, H-4); 3.70 (2 H, ABq, $J = 16$ Hz, PhCH_2-); 5.05 (1 H, d, $J = 5.5$ Hz, H-6); 5.60 (1 H, d, $J = 5.5$ Hz, H-7); m/z (negative ESI MS) = 331 (M-H).

Incubation of penicillin G (10)

DAOCS (6.14 mg, 119 units/mg, 730 units) and penicillin G (**10**, 7.56 mg, 20 μmol) were incubated in a final volume of 2 ml (Shibata *et al*., 1996) for two hours. The reaction was quenched with 5 ml of acetone, which was removed *in vacuo* before freeze-drying. ^{1}H NMR (500 MHz) analyses implied a ca 20-30% conversion of penicillin G (**10**) to G-7-ADCA (**11**), as judged by integration of the resonance at 5.60 p.p.m. against TSP. Purification of the crude incubation mixture by HPLC (as above with 10% (v/v) methanol in the eluent) gave G-7-ADCA (**11**) (45 μg) with a retention volume of 23.2-26.4 ml. ^{1}H NMR and ESI MS analyses were the same as those reported above for synthetic (**11**).

Kinetic assays

Protein (10 μl) was mixed with 10 μl of 10 × stock solution of cofactors (500 mM $(NH_4)_2SO_4$, 10 mM 2-oxoglutarate, 20 mM DTT, 10 nM ascorbate, 20 mM $FeSO_4$, NaOH to pH 7.5 in 50 mM Tris-HCl, p 7.5) and incubated at ambient temperature for two minutes. The mixture was diluted with 70 μl of 50 mM Tris-HCl (pH 7.5) and the reaction initiated by addition of 1.0 mM penicillin N (**1**, 10 μl). After 5 minutes methanol (100 μl) was added and 50 or 100 μl was used to measure the DAOC present using the holed-plate method with *E. coli* ESS as the indicator organism (Baldwin *et al*., 1987a,b). Plates were calibrated using DAOC (0.5-1.0 nmol). Alternatively, DAOC (**2**) was quantified using anion-exchange HPLC (Morgan *et al*., 1994; Shibata *et al*., 1996). Protein concentrations were determined by the method of Bradford (1976) using BSA as a calibration standard.

Kinetic parameters for penicillin G (**10**) were determined with 1, 2, 3, 4, 5, 6, 8 and 10 mM substrate using 18.8 μg DAOCS/assay in a total volume of 200 μl. After quenching the reaction with 200 μl methanol, 200 μl of water was added. Samples were centrifuged and analysed by HPLC (150 μl injections, as above using 15% (v/v) methanol in the eluent). Product was quantified by peak height at 0.05 AUFS using synthetic G-7-ADCA (**11**, 0.5-3.5 nmol) as standard. Kinetic parameters (±SE) were determined using Leonora by directly fitting of the data to the appropriate kinetic expression following initial graphical analysis.

Preliminary experiments with metal ions used the HPLC assay with penicillin N (**1**) as substrate. Enzyme was preincubated for two minutes with cofactors with the appropriate metal ion at 2 mM final concentration replacing Fe(II). Analysis of metal ions as potential inhibitors was performed by the same method using the standard cofactor mixture with Fe(II).

UV-visible spectra were recorded using a Phillips Pye-Unicam 8800 UV-visible spectrophotometer in 10 mM Na_2HPO_4-HCl (pH 7.0).

DTNB titration of DAOCS

DAOCS (ca 1 mg) in 200 μl of 50 mM Tris-HCl(pH 7.5) was incubated on ice with 2.5 mM DTT for two hours 15 minutes. The sample was diluted to 500 μl and exchanged into 50 mM Tris-HCl (pH 8.0) with a NAP-5 column. The sample was diluted to 4 ml and 0.7 ml was assayed at A_{412} (Habeeb, 1974) in the presence or absence of 2% SDS (w/v) with 1 mM DTNB.

Dynamic laser light scattering

Dynamic laser light scattering measurements were performed in a DynaPro-801 TC instrument at 8-37 °C using DAOCS (1 mg/ml) in 10 mM Hepes-NaOH (pH 7.0) Samples containing iron(II) were prepared and measured under anaerobic conditions.

Preparation and analysis of EXAFS samples

A crude extract of *E. coli* BL21 (DE3)/pML1 was prepared and purified by anion-exchange chromatography on DEAE Sepharose® FF and gel filtration chromatography as described above. Final purification was achieved with Mono Q® 16/10 column chromatography using a 0-0.4 M NaCl gradient over 13 ml. Purified DAOCS were exchanged into 10 mM Tris-HCl, 0.3 mM (NaN_3 (pH 7.5) and concentrated to 74 mg/ml (ca 2.15 mM). Iron(II) sulphate (100 mM, 5 μl) or $FeSO_4$ and potassium 2-oxoglutarate (200 mM, 2.5 μl) were added to 250 μl of enzyme under anaerobic conditions and frozen in liquid nitrogen in the EXAFS cell.

The EXAFS data (Randall *et al*., 1993) were recorded at ca 80 K on station 8.1 of the CCLRC Daresbury SRS, operated at 2 GeV with an average current of 150 mA, using a liquid nitrogen-cooled cold finger. Twelve scans were recorded and averaged for each sample. The Fe K-edge spectra were calibrated relative to the first peak in the derivative for an iron foil Spectrum at 7112 eV. Spectra were analysed, including multiple scattering, in EXCURV92 (Binsted *et al*., 1991) using exact wave theory (Lee & Pendry, 1975; Gurman *et al*., 1984, 1986). Phase shifts were calculated *ab initio* using Hedin-Lundqvist potentials (Hedin & Lundqvist, 1969). Theoretical fits were generated by adding shells of scatterers around the central iron atom and iterating the bond lengths and Debye-Waller type parameters to achieve the optimum fit to the experimental data. To reduce the number of parameters used to interpret the EXAFS, the occupation number of each shell of backscattering atoms was fixed at an integer value and a restrained refinement approach (Binsted *et al*., 1992) used to treat the backscattering of

the imidazole rings of the histidine ligands. Thus, these groups were each treated as single units constrained at the known geometry, including multiple scattering pathways and keeping Debye-Waller parameters the same for atoms at similar distances from the metal (Binsted *et al.*, 1992). Backscattering from the 2-oxoglutarate group was similarly treated by restrained refinement using the geometry previously determined for sodium 2-oxoglutarate (Lis & Matuszewski, 1984).

Crystallization of DAOCS

Crystals of DAOCS were grown by vapour-diffusion using the hanging drop method at ca 20 °C. The precipitating solution consisted of 100 mM Hepes-NaOH (pH 7.0), 5 mM potassium 2-oxoglutarate and 1.6-1.7 M $(NH_4)_2SO_4$. Drops (3 µl) consisted of 55 mM Hepes-NaOH (pH 7.0), 2.5 mM potassium 2-oxoglutarate and 0.8-0.85 M $(NH_4)_2SO_4$. Selenomethionyl-DAOCS could only be crystallized under these conditions in the anaerobic glove box with dioxygen levels maintained at 0.1-0.3 p.p.m. throughout. These crystals were used to determine the structure of DAOCS (Valegård *et al.*, 1998) using isomorphous replacement and a detwinning strategy (A.C. Terwisscha van Scheltinga *et al.*, unpublished results). An independent structure of the DAOCS, 2-oxoglutarate complex was also determined to 2.5 Å by isomorphous replacement (K. Harlos & M. D. Lloyd, unpublished results). Both structures were used during the analysis of the DAOCS reaction mechanism.

Accession numbers

Co-ordinates and structure factors have been deposited with the Protein Data Bank (entries 1dcs and r1dcssf for apoenzyme, 1rxf and r1rxfsf for the iron complex, and 1rxg and r1rxgsf for the iron, 2-oxoglutarate complex).

Acknowledgements

We thank Mr J. Pitt and Mr J. Keeping for technical assistance, Drs R. T. Aplin and R. P. Brown for ESI MS analysis, and Mr A. C. Willis for sequencing and peptide analysis. Drs D. Staunton, J. Endicott and E. Y. Jones (Department of Biochemistry, University of Oxford) are gratefully thanked for advice on the preparation of selenomethionine derivatives. The Director of Daresbury Laboratory is thanked for provision of beam time and computational facilities. This research was supported by the EPSRC, BBSRC and MRC (grant number 43/IR2523-1), the E.U. Biotechnology Programme (grant number BIO4-CT96-0126) and the Swedish Research Councils NFR and MFR.

References

Baldwin, J. E. & Abraham, E. P. (1988). The biosynthesis of penicillins and cephalosporins. *Nature Prod. Rep.* **5**, 129-145.

Baldwin, J. E. & Bradley, M. (1990). Isopenicillin N synthase: mechanistic studies. *Chem. Rev.* **90**, 1079-1088.

Baldwin, J. E. & Schofield, C. J. (1992). The biosynthesis of β-lactams. In *The Chemistry of β-lactams* (Page, M. I., ed), chap. 1, pp. 1-78, Blackie Academic and Professional, London.

Baldwin, J. E., Abraham, E. P., Adlington, R. M., Bahadur, G. A., Chakravarti, B., Domayne-Hayman, B. R., Field, L. D., Flitsch, S. L., Jayatilake, G. S., Spakovskis, A., Ting, H.-H., Turner, N. L., White, R. L. & Usher, J. J. (1984). Penicillin biosynthesis: active site mapping with aminoadipoylcysteinylvaline variants. *J. Chem. Soc. Chem. Commun.*, 1225-1227.

Baldwin, J. E., Adlington, R. M., Crouch, , Schofield, C. J. & Ting, H-H. (1987a). Stepwise hydrogen removal in the enzymic ring expansion of penicillin N to deacetoxycephalosporin C. *J. Chem. Soc. Chem. Commun.*, 1654-1656.

Baldwin, J. E., Adlington, R. M., Coates, J. B., Crabbe, M. J. C., Crouch, N. R., Keeping, J. W., Knight, G. C., Schofield, C. J., Ting, H.-H., Vallejo, C. A., Thorniley, M. & Abraham, E. P. (1987b). Purification and initial characterisation of an enzyme with deacetoxycephalosporin C synthetase and hydroxylase activities. *Biochem. J.* **245**, 831-841.

Baldwin, J. E., Adlington, R. M., Kang, T. W., Lee, E. & Schofield, C. J. (1988). The ring expansion of penicillins to cephams: a possible biomimetic process. *Tetrahedron*, **44**, 5953-5957.

Baldwin, J. E., Schofield, C. J. & Smith, B. D. (1990). Side-chain specificity in the enzymatic synthesis of penicillins. *Tetrahedron*, **46**, 3019-3028.

Baldwin, J. E., Adlington, R. M., Crouch, N. R., Knight, G., Schofield, C. J., Turner, N. J. & in part Aplin, R. T. (1991). Cephalosporin biosynthesis: a branched pathway sensitive to an isotope effect. *Tetrahedron*, **47**, 1651-1654 and references therein.

Barlow, J. N., Baldwin, J. E., Clifton, I. J., Gibson, E., Hensgens, C. M. H., Hajdu, J., Hara, T., Hassan, A., John, R., Lloyd, M. D., Roach, P. L., Prescott, A., Robinson, J. K., Zhang, Z.-H. & Schofield, C. J. (1997). Studies on non-haem ferrous-dependent oxygenases and oxidases. *Biochem. Soc. Trans.* **25**, 86-90.

Binsted, N., Campbell, J. W., Gurman, S. J. & Stephenson, P. C. (1991). *Daresbury Laboratory EXCURV92 program.*

Binsted, N., Strange, R. W. & Hasnain, S. S. (1992). Constrained and restrained refinement in EXAFS data analysis with curved wave theory. *Biochemistry*, vol. 31, 12117-12125.

Borovok, I., Landman, O., Kreisberg-Zakarin, R., Aharonowitz, Y. & Cohen, G. (1996). Ferrous active site of isopenicillin N synthase: genetic and sequence analysis of the endogenous ligands. *Biochemistry*, **35**, 1981-1987.

Bradford, M. M. (1976). A rapid and sensitive method for the quantitation of microgram quantities of protein utilizing the principle of protein-dye binding. *Anal. Biochem.* **72**, 248-254.

Chauvette, R. R., Pennington, P. A., Ryan, C. W., Cooper, R. D. G., José, F. L., Wright, I. G., Van Heyningen, E. M. & Huffman, G. W. (1971). Chemistry of cephalosporin antibiotics. XXI. Conversion of penicillins to cephalexin. *J. Org. Chem.* **36**, 1259-1267.

Colvin, E. W. (1992). In *The Chemistry of the β-Lactam Antibiotics* (Page, M. I., ed.), pp. 336-340, Blackie Academic and Professional, London.

Cooper, R. D. G. (1993). The enzymes involved in the biosynthesis of penicillins and cephalosporins. Their structure and function. *Bioorg. Med. Chem.* **1**, 1-17.

Crawford, L., Stepan, A. M., McAda, P. C., Rambosek, J. A., Condor, M. J., Vinci, V. A. & Reeves, C. J. (1995). Production of cephalosporin intermediates by feeding adipic acid to recombinant *Penicillium chrysogenum* strains expressing ring expansion activity. *Bio/Technol.* **13**, 58-62.

Dotzlaf, J. E. & Yeh, W.-K. (1989). Purification and properties of deacetoxycephalosporin C synthase from recombinant *Escherichia coli* and its comparison with the native enzyme purified from *Streptomyces clavuligerus*. *J. Biol. Chem.* **264**, 10219-10227.

Gurman, S. L., Binsted, N. & Ross, I. (1984). A rapid, exact, curved wave theory for EXAFS calculations. *J. Phys. C: Sol. St. Phys.* **17**, 143-151.

Gurman, S. J., Binsted, N. & Ross, I. (1986). A rapid, exact, curved wave theory for EXAFS calculations II. The multiple scattering contributions. *J. Phys. C: Sol. St. Phys.* **19**, 1845-1861.

Habeeb, A. F. S. A. (1974). Reaction of protein sulfhydryl groups with Ellman's reagent. In *Methods in Enzymol* (Hirs, C. H. W. & Timersheff, S. N., eds), vol. 25, pp. 457-464, Academic Press, London.

Hedin, L. & Lundqvist, S. (1969). Effects of electron-electron and electron-phonon interactions on the one-electron states of solids. *Solid State Phys.* **23**, 1-181.

Hegg, E. L. & Que, L. (1997). The 2-His-1-carboxylate facial triad. An emerging structural motif in mononuclear non-heme iron(II) enzymes. *Eur. J. Biochem.* **250**, 625-629.

Hendrickson, W. A., Horton, J. R. & LeMaster, D. M. (1990). Selenomethionyl proteins produced for analysis by multiple anomalous diffraction (MAD): a vehicle for direct determination of three dimensional structure. *EMBO J.* **9**, 1665-1672.

Holme, E. (1975). A kinetic study of thymine hydroxylase from *Neurospora crassa*. *Biochemistry*, **14**, 4999-5003.

Kovacevic, S., Weigal, B. J., Tobin, M. B., Ingolia, T. & Miller, J. R. (1989). Cloning, characterisation and expression in *Escherichia coli* of the *Streptomyces clavuligerus* gene encoding deacetoxycephalosporin C synthase. *J. Bacteriol.* **171**, 754-760.

Lee, P. A. & Pendry, J. B. (1975). Theory of the extended X-ray absorption fine structure. *Phys. Rev.* **B11**, 2795-2811.

Lis, T. & Matuszewski, J. (1984). The structures of α-ketoglutaric acid (I), $C_5H_6O_5$, sodium hydrogen α-ketoglutarate (II), $Na + C_5H_5O_5$-, and potassium hydrogen α-ketoglutarate (III), $K + C_5H_5O_5$-. *Acta Crystallog. sect. C*, **40**, 2016-2019.

Lloyd, M. D. (1996). Fast staining and destaining of sodium dodecyl sulphate polyacrylamide gels. *Anal. Biochem.* **241**, 139-140 and references therein.

Matthews, B. W. (1968). Solvent content of protein crystals. *J. Mol. Biol.* **33**, 491-497.

Morgan, N. (1994). Genetic engineering of cephalosporin biosynthesis. D.Phil. thesis, University of Oxford.

Morgan, N., Pereira, I. A. C., Andersson, I. A., Adlington, R. M., Baldwin, J. E., Cole, S. C. J., Crouch, N. P. & Sutherland, J. D. (1994). Substrate specificity of recombinant *Streptomyces clavuligerus* deacetoxycephalosporin C synthase. *Bioorg. Med. Chem. Letters*, **4**, 1595-1600.

Morin, R. B., Jackson, B. G., Mueller, R. A., Lavagnino, E. R., Scanlon, W. B. & Andrews, S. L. (1963). Chemistry of cephalosporin antibiotics. III. Chemical correlation of penicillins & cephalosporin antibiotics. *J. Am. Chem. Soc.* **85**, 1896-1897.

Myllyharju, J. & Kivirikko, K. I. (1997). Characterization of the iron- and 2-oxoglutarate-binding sites of prolyl 4-hydroxylase. *EMBO J.* **16**, 1173-1180.

Pang, C.-P., White, R. L., Abraham, E. P., Crout, D. H. G., Lutstorf, M., Morgan, P. J. & Derome, A. E. (1984). Stereochemistry of the incorporation of valine methyl groups into methylene groups in cephalosporin C. *Biochem. J.* **222**, 777-788.

Pappa, H. S., Steward, A. E. & McDonald, N. Q. (1996). Incorporating anomalous scattering centres into macromolecules. *Curr. Opin Struct. Biol.* **6**, 611-616.

Pavel, E. G., Zhou, L., Busby, R. W., Gunsior, M., Townsend, C. A. & Solomon, E. I. (1998). Circular dichroism and magnetic circular dichroism spectroscopic studies of the non-heme ferrous active site in clavaminate synthase and its interaction with α-ketoglutarate cosubstrate. *J. Am. Chem. Soc.* **120**, 743-753.

Prescott, A. G. (1993). A dilemma of dioxygenases (or where biochemistry and molecular biology fail to meet). *J. Exp. Bot.* **44**, 849-861.

Que, L. & Ho, R. Y. N. (1996). Dioxygen activation by enzymes with mononuclear non-heme iron active sites. *Chem. Rev.* **96**, 2607-2624.

Randall, C. R., Zang, Y., True, A. E., Que, L., Jr, Charnock, J. M., Garner, C. D., Fujishima, Y., Schofield, C. J. & Baldwin, J. E. (1993). X-ray absorption studi on the ferrous active site of isopenicillin N synthase and related model complexes. *Biochemistry*, **32**, 6664-6673.

Roach, P. L., Clifton, I. J., Fülöp, V., Harlos, K., Barton, G. J., Hajdu, J., Andersson, I., Schofield, C. J. & Baldwin, J. E. (1995). Crystal structure of isopenicillin N synthase is the first from a new structural family of enzymes. *Nature*, **375**, 700-704.

Roach, P. L., Clifton, L., Hensgens, C. M. H., Shibata, N., Schofield, C. J., Hajdu, J. & Baldwin, J. E. (1997). Structure of isopenicillin N synthase complexed with substrate and the mechanism of penicillin formation. *Nature*, **387**, 827-830.

Sambrook, L., Fritsch, E. F. & Maniatis, T. (1989). *Molecular Cloning: A Laboratory Manual* (Nolan, C., ed.), 2nd edit., Cold Spring Harbor Laboratory Press, Cold Spring Harbor, NY.

Sami, M., Brown, T. J. N., Roach, P. L., Schofield, C. J. & Baldwin, J. E. (1997). Glutamine-330 is not essential for activity in isopenicillin N synthase from *Aspergillus nidulans*. *FEBS Letters*, **405**, 191-194.

Schofield, C. J., Baldwin, J. E., Byford, M. F., Clifton, I., Hajdu, J. & Roach, P. L. (1997). Proteins of the penicillin biosynthesis pathway. *Curr. Opin. Struct. Biol.* **7**, 857-864.

Shibata, N., Lloyd, M. D., Baldwin, J. E. & Schofield, C. J. (1996). Adipoyl-6-aminopenicillanic acid is a substrate for deacetoxycephalosporin C synthase (DAOCS). *Bioorg. Med. Chem. Letters*, **6**, 1579-1584 and references therein.

Townsend, C. A., Theis, A. B., Neese, A. S., Barrabee, E. B. & Poland, D. (1985). Stereochemical fate of chiral-methyl valine in the ring expansion of penicillin N to deacetoxycephalosporin C. *J. Am. Chem. Soc.* **107**, 4760-4767.

Valegård, K., Terwisscha Van Scheltinga, A. C., Lloyd, M. D., Hara, T., Ramaswamy, S., Perrakis, A., Thompson, A., Lee, H.-J., Baldwin, J. E., Schofield, C. J., Hajdu, J. & Andersson, I. (1998). Structure of a cephalosporin synthase. *Nature*, **394**, 805-809.

Whiting, A. K., Que, L., Saari, R. E., Hausinger, R. P., Fredrich, M. A. & McCracken, J. (1997). Metal co-

ordination environment of a Cu(II)-substituted α-keto acid-dependent dioxygenase that degrades the herbicide 2,4-D. *J. Am. Chem. Soc.* **119**, 3413-3414.

Zhang, Z.-E., Barlow, J. N., Baldwin, J. E. & Schofield, C. J. (1997). Metal-catalysed oxidation and mutagenesis studies on the iron(II) binding site of 1-aminocyclopropane-1-carboxylate oxidase. *Biochemistry*, **36**, 15999-16007.

Edited by D. C. Rees

(Received 30 July 1998; received in revised form 15 January 1999; accepted 16 January 1999)

Article No. jmbi.1999.2652 available online at http://www.idealibrary.com on IDEAL J. Mol. Biol. (1999) 287, 961–968

JMB

Surface Crystallisation of the Plasma Membrane H^+-ATPase on a Carbon Support Film for Electron Crystallography

Manfred Auer[1,3]*, Gene A. Scarborough[2] and Werner Kühlbrandt[1]

[1]*Max-Planck-Institut für Biophysik, Abt. Strukturbiologie, Heinrich-Hoffmann-Str. 7 D-60528, Frankfurt am Main Germany*

[2]*Department of Pharmacology University of North Carolina Chapel Hill, NC 27599, USA*

[3]*European Molecular Biology Laboratory, Meyerhofstr. 1 D-69117 Heidelberg, Germany*

**Corresponding author*

Large two-dimensional crystals of H^+-ATPase, a 100 kDa integral membrane protein, were grown directly onto the carbon surface of an electron microscope grid. This procedure prevented the fragmentation that is normally observed upon transfer of the crystals from the air-water interface to a continuous carbon support film. Crystals grown by this method measure ~5 μm across and have a thickness of ~240 Å. They are of better quality than the monolayers previously obtained at the air-water interface, yielding structure factors to at least 8 Å in-plane resolution by electron image processing. Unlike most other two-dimensional crystals of membrane proteins they do not contain a lipid bilayer, but consist of detergent-protein micelles of H^+-ATPase hexamers tightly packed on a trigonal lattice. The crystals belong to the two-sided plane group *p*321 ($a = b = 165$ Å), containing two layers of hexamers related by an in-plane axis of 2-fold symmetry. The protein is in contact with the carbon surface through its large, hydrophilic 70 kDa cytoplasmic portion, yet due to the presence of detergent in the crystallizing buffer, the hydrophobicity of the carbon surface does not appear to affect crystal formation. Surface crystallisation may be a useful method for other proteins which form fragile two-dimensional crystals, in particular if conditions for obtaining three-dimensional crystals are known, but their quality or stability is insufficient for X-ray structure determination.

Keywords: surface crystallisation; 2D crystal; electron crystallography; membrane protein; P-type H^+-ATPase

Introduction

In recent years, electron microscopy of two-dimensional (2D) crystals has developed into a viable alternative to X-ray crystallography for determining the structure of large biological macromolecules that do not yield highly ordered three-dimensional (3D) crystals. This is often the case with membrane proteins, and for this reason electron microscopy has been particularly successful as a tool in membrane biology. To date, atomic models of two membrane proteins have been derived by electron crystallography: bacteriorhodopsin (Henderson *et al.*, 1990) and the plant light-harvesting complex LHC II (Kühlbrandt *et al.*, 1994). Several other membrane protein structures determined at intermediate resolution (6-9 Å) have revealed the arrangement of membrane-spanning α-helices: these include aquaporin (Cheng *et al.*, 1997; Walz *et al.*, 1997; Li *et al.*, 1997) at 6 Å, rhodopsin (Unger *et al.*, 1997), Ca^{2+}-ATPase (Zhang *et al.*, 1998a) and H^+-ATPase (Auer *et al.*, 1998) at 8 Å, and the nicotinic acetylcholine receptor at 9 Å resolution (Unwin, 1995).

With the exception of the H^+-ATPase which is discussed here, all these 3D structures were determined from sheet-like or tubular 2D crystals in which the membrane protein is embedded in a lipid bilayer. A few membrane proteins naturally form 2D crystals (bacteriorhodopsin, gap junctions), but some can be induced to crystallise *in situ* by rearrangement in the lipid bilayer of isolated membranes (acetylcholine receptor, rhodopsin, Ca^{2+}-ATPase). A widely used procedure for generating 2D crystals is the reconstitution of the purified, detergent-solubilised membrane protein

Present adress: M. Auer, Skirball Institute of Biomolecular Medicine, New York University Medical Center, 540 First Avenue, New York, NY10016, USA.

E-mail address of the corresponding author: auer@saturn.med.nyu.edu

0022-2836/99/150961–08 $30.00/0

into lipid sheets or vesicles (for a review, see Kühlbrandt, 1992). Detergent is removed either by dialysis (Kühlbrandt, 1992; Jap *et al*., 1992) or by absorption to BioBeads (Rigaud *et al*., 1997). This approach has yielded highly ordered 2D crystals of membrane proteins which do not have large extramembraneous domains and which therefore rely mainly on hydrophobic protein-protein or lipid-protein interactions in the lipid bilayer, such as LHC-II, bacteriorhodopsin, and aquaporin. Membrane proteins with large hydrophilic domains tend to form 3D crystals more readily due to the potential of the extramembrane portions for hydrophilic crystal contacts. A number of 3D membrane protein crystals have yielded structures at near-atomic resolution by X-ray crystallography (Deisenhofer *et al*., 1984; Weiss *et al*., 1991; Cowan *et al*., 1992; Iwata *et al*., 1995; Tsukihara *et al*., 1995; McDermott *et al*., 1995; Koepke *et al*., 1996; Song *et al*., 1996; Yu *et al*., 1997; Pebay-Peroula *et al*., 1997; Doyle *et al*., 1998; Zhang *et al*., 1998b). Unfortunately it is not unusual for 3D crystals of membrane proteins to be poorly ordered, or too small for X-ray diffraction. For electron crystallography on the other hand, small crystalline arrays of less than 1 μm are, in principle, sufficient for a 3D structure determination at high resolution (Henderson, 1995), provided that the crystals are thin enough, and ideally form monolayers. Electron image processing can correct small crystal distortions and is therefore uniquely able to extract useful structural information from imperfect crystals having long-range disorder (Henderson *et al*., 1986).

We have used electron microscopy to study the integral membrane protein H^+-ATPase from the *Neurospora crassa* plasma membrane. Drops of solution for growing 3D crystals diffracting X-rays to ~9 Å resolution (Scarborough, 1994) were found to produce crystalline monolayers of protein hexamers at the air-water interface (Cyrklaff *et al*., 1995). Such 2D crystals grown in or transferred to the holes of a holey carbon film yielded a projected structure of the H^+-ATPase hexamer at 10.3 Å resolution (Cyrklaff *et al*., 1995). However, in order to obtain a 3D density map from tilted samples, it was necessary to transfer these crystals onto a continuous carbon support film, to avoid problems of crystal curvature and specimen charging. These effects made it difficult to collect good images of unsupported 2D crystals for structure determination, especially at large tilt angles. Here, we describe a method by which 2D crystals of the H^+-ATPase suitable for 3D structure determination by electron crystallography are grown directly on the carbon film of a support grid. By this method, the problems mentioned above are at least partially overcome. This has enabled us to determine the 3D structure of the *N. crassa* plasma membrane H^+-ATPase at 8 Å resolution (Auer *et al*., 1998).

Results

The crystalline sheets of H^+-ATPase hexamers forming at the air-water interface of crystallisation drops (Cyrklaff *et al*., 1995) seemed highly promising for the determination of the 3D structure of this important ion pump by electron microscopy and image processing. However, the sheets were extremely fragile which made it difficult to transfer them onto a continuous carbon support film, an important prerequisite for 3D data collection. The transfer often resulted in complete disruption of the crystal into small fragments as a result of surface forces (Figure 1). In addition, the crystals tended to stack, apparently forming thin 3D crystals, which were difficult to distinguish from true 2D crystals in unsupported, frozen-hydrated specimens. By growing the crystals directly on the carbon film surface, we were able to overcome both problems.

Preliminary experiments with holey carbon films incubated on crystallisation drops had shown that 2D crystals forming in the holes occasionally extended onto the carbon film. Initial crystallisation trials in which droplets were incubated on continuous carbon film for several hours resulted in mosaics of small crystalline arrays which were visible in negative stain. A pre-evaporation step of leaving the droplet to evaporate in air at 4 °C for ten minutes before placing the grid on it, followed by incubation in the sealed well of a Linbro plate for eight to 12 hours, resulted in the formation of large crystals (~15-20 μm). These were mostly stepped multilayers (Figure 2). The length of the steps indicated that in-plane crystal growth was faster than in the perpendicular direction. By varying conditions between these two extremes it was possible to devise a procedure which reproducibly yielded sufficiently large 2D crystals with a thick-

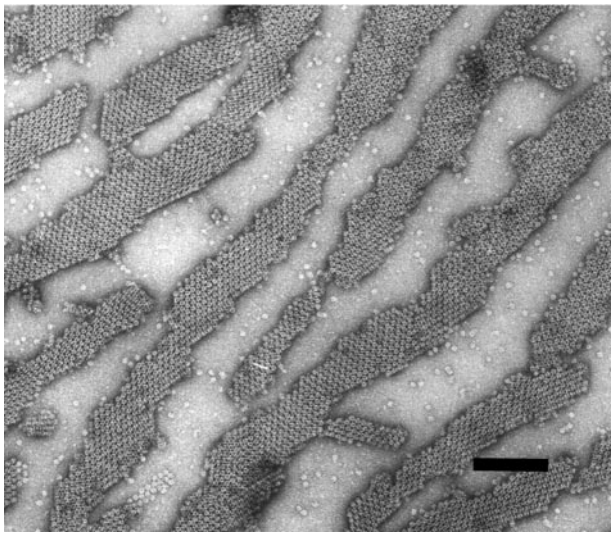

Figure 1. Crystalline arrays of *N. crassa* H^+-ATPase grown at the air-water interface fragmented during transfer onto a continuous carbon support film. The scale bar represents 200 nm.

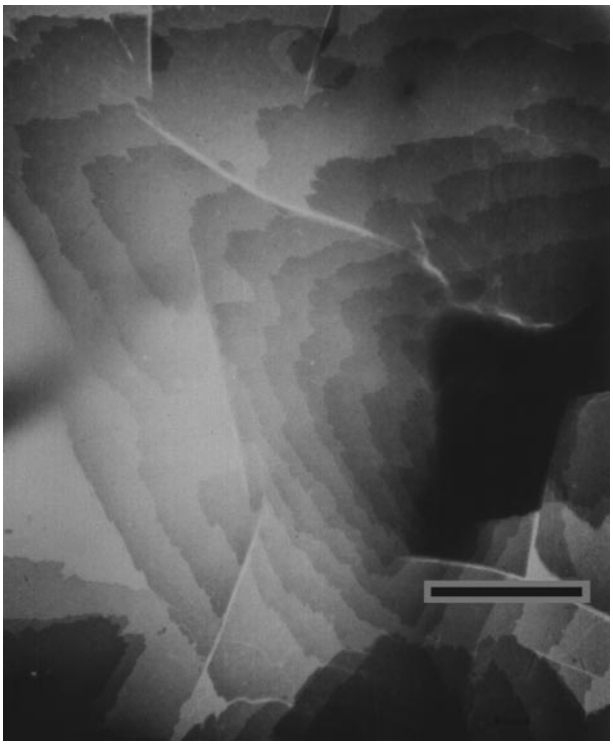

Figure 2. Thin three-dimensional crystals of H^+-ATPase grown on the surface of a carbon support film. Crystals show density steps indicating that the rate of formation in the plane of the support film is higher than in the perpendicular direction. The scale bar represents 5 μm.

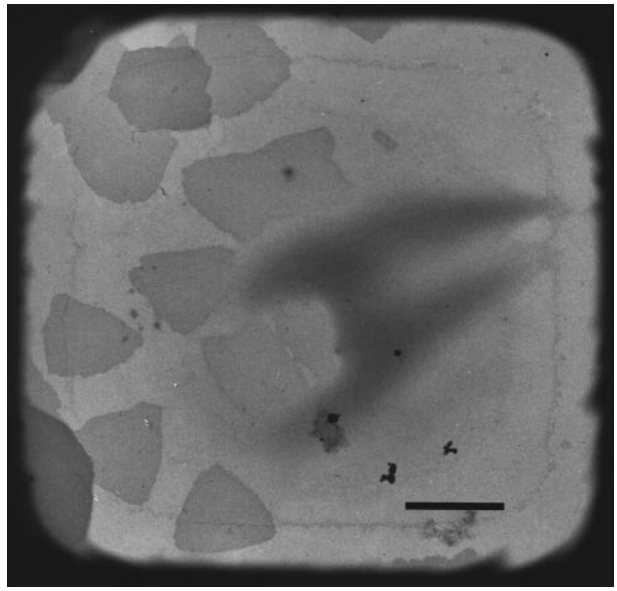

Figure 3. Two-dimensional crystals of H^+-ATPase grown on carbon film supported by a 400 mesh electron microscope grid. One whole grid square is shown. The 2D crystals consisting of two layers of ATPase hexamers have a characteristic triangular shape. Prolonged crystallisation times lead to the formation of darker multilayers. The scale bar represents 5 μm.

ness of one unit cell. The formation of multilayers was avoided almost completely by omitting the ten minute pre-evaporation step, apparently due to the presence of fewer nucleation sites and slower crystal growth. The final size of the crystals was strongly time-dependent. As expected, shorter incubation times yielded smaller crystals, whereas longer incubation periods produced crystals of up to ~10 μm size, but increased the risk of multilayer formation. With the protein preparation used for most of the experiments, an incubation time of ca two hours proved to be optimal, yielding large numbers of single crystals of a characteristic triangular shape that grew routinely to a size of ~5 μm (Figure 3).

Upon variation of the crystallisation conditions we observed that crystals could also be obtained with lower concentrations of ammonium sulphate, e.g. 50 mM, but not with 25 mM or 5 mM. The 2D crystals grew at concentrations of polyethylene glycol (PEG) 4000 between 8% and 12%, but not 4% (10.5% was optimal) as well as with 10.5% PEG 8000 instead of PEG 4000, but not with 10.5% PEG 400 or PEG 1000. At higher detergent concentrations (~10 mg/ml instead of 1.28 mg/ml), 2D crystal formation was not observed. An increase of the temperature during crystallisation from 4 °C to 20 °C resulted in 2D crystals that curled at the edges, and when obtained at the air-water interface, the crystals even rolled into tubes which were open at both ends, which distinguished them from tubular crystals of membrane proteins in lipid bilayers. It is interesting to note that 2D crystals were also found at protein concentrations as low as 0.1 mg/ml under otherwise similar crystallisation conditions.

The thickness of the electron microscope grid was an important factor influencing the number of crystals found on a grid. In this respect, the use of gold-coated copper electron microscope grids proved to be an advantage as they are thinner than conventional grids and thus facilitate the contact between the carbon film and the drop surface. The hydrophobicity of the carbon surface did not appear to affect crystal formation, as 2D crystals grew equally well on carbon films rendered hydrophobic by baking and on films that had been made hydrophilic by glow-discharging in air or amylamine (results not shown). This was probably due to the presence of detergent in the crystallisation solution which should cover the carbon surface and neutralise any differences in hydrophobicity.

Micrographs of 2D crystals routinely yielded diffraction spots to 8 Å in-plane resolution after correction for lattice distortions. Figure 4 shows the Fourier transform of one such image in which some reflections are visible to ~6 Å. Surprisingly, phase comparison of symmetry-related reflections did not indicate *p*6 symmetry as in the case of the single-layer sheets that formed at the air-water interface (Cyrklaff *et al.*, 1995). Instead, some images of 2D crystals grown on carbon film

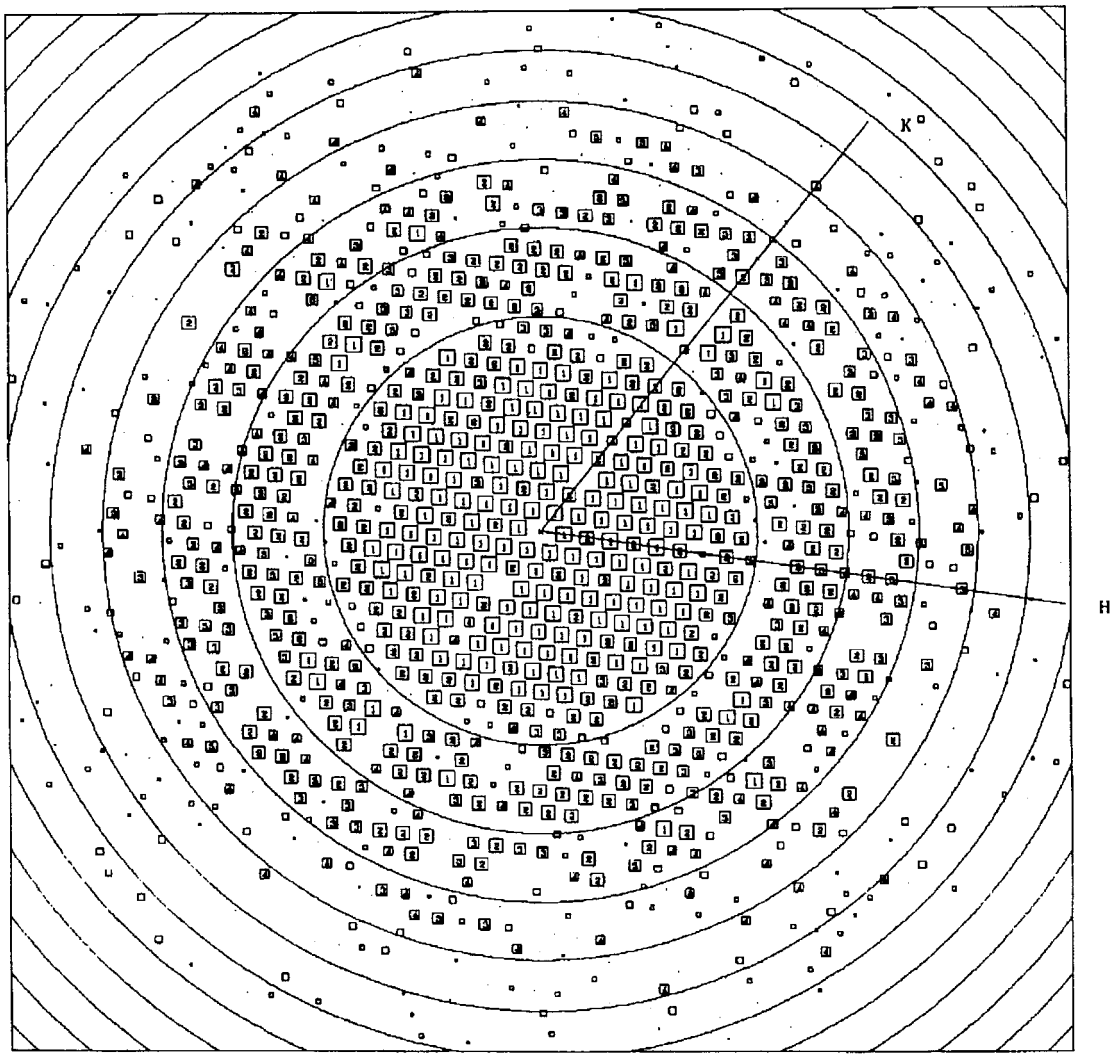

Figure 4. Plot of the Fourier transform of an image of a 2D crystal of the H^+-ATPase with apparent *p*321 symmetry, showing positions of observable structure factors as squares on reciprocal lattice positions. Large squares and small numbers indicate reflections of high signal/noise ratio, as described by Henderson *et al*. (1986). Concentric lines indicate the zero positions of the contrast transfer function. Arrows indicate the direction of the reciprocal lattice vectors *h* and *k*. The edge of the plot corresponds to a resolution of 6.7 Å.

showed *p*321 symmetry, with phase residuals of 20-25° (90° is random). In many others, the symmetry was less obvious, although it was unusually close to *p*321. This meant that the crystals grown on the carbon film were not single layers of H^+-ATPase hexamers, but consisted of at least two such layers. We therefore combined two *p*6 layers from our earlier projection map (Cyrklaff *et al*., 1995) into a *p*321 projection and compared this with the experimentally determined projection map of a carbon surface-grown crystal. The close agreement between the two maps suggested that at least those substrate-grown crystals that showed clear *p*321 symmetry were composed of two layers of hexamers, related by an in-plane 2-fold axis (data not shown).

This presented three likely explanations for the imperfect *p*321 symmetry observed in a substantial fraction of the images: either it was due to a small lateral shift of one layer from the *p*321 symmetry-related position, or to the presence of additional layers breaking the *p*321 symmetry, or to a small tilt of the crystal resulting in an apparent loss of the *p*321 projection symmetry. The comparison of each of these images to a combined set of amplitudes and phases used for calculating the 3D map of the H^+-ATPase (Auer *et al*., 1998) indicated that the deviations were due to small crystal tilts, in the range of ~3° to 7°, even though the grid was nominally untilted. When these tilt angles were taken into account, the phases from images without clear *p*321 projection symmetry merged readily into the data set, resulting in phase residuals of 20° to 30° (90° being random). With most 2D crystals, such small tilts would not result in an obvious deviation from the projection symmetry. Due to the unusual thickness (~240 Å) of the H^+-ATPase 2D

crystals, however, the amplitudes and phases of Fourier components vary rapidly in z^* direction, causing an apparent breakdown of the projection symmetry at tilt angles of less than 10°.

Interestingly, the carbon film in the vicinity of a crystal was covered with a monolayer of closely packed H^+-ATPase hexamers. These were visible in negative stain, and by cryomicroscopy as a characteristic pattern of gas bubbles produced by radiation damage. Surprisingly, this surrounding layer did not appear to be crystalline, as optical diffraction of electron micrographs of such areas indicated little, if any order. In contrast, the single layers that had occasionally been found at the air-water interface were clearly crystalline and diffracted to ~12 Å (Cyrklaff *et al*., 1995).

Discussion

Because the protein preparation contains little, if any, lipid (Chadwick *et al*., 1987; G.A.S., unpublished results) and no lipid was added to the crystallisation mixture, there can be no lipid bilayer in the surface crystals of the H^+-ATPase. The 2D crystals are clearly not held together by hydrophobic interactions between lipids and proteins which stabilise 2D crystals of most other membrane proteins, and are therefore likely to be arrays of detergent-protein mixed micelles. This was confirmed by the 3D structure of the plasma membrane H^+-ATPase at 8 Å resolution which revealed that the crystals consisted of tightly packed ATPase hexamers, each surrounded by a toroidal micelle of the detergent dodecyl-β-D-maltoside. The absence of a lipid bilayer explains why the crystals are so susceptible to disruption by the interfacial forces which occur when they are transferred onto electron microscope grids.

Growing the crystals on the carbon film surface was essential for collecting a 3D data set, as it avoided the fragmentation of the crystals and minimized beam-induced movement. The experimental design resembles a conventional hanging drop vapour diffusion experiment, except that a carbon-coated electron microscope grid covers the drop surface. We used conditions which had reproducibly yielded 3D crystals of the H^+-ATPase (Scarborough, 1994). The resulting 2D crystals were harvested after a few hours, as longer incubation times resulted in the formation of multilayers which are difficult to deal with in electron crystallography.

The double-layered 2D crystals of the ATPase obtained by surface crystallisation were larger and more highly ordered than the single crystals obtained at the air-water interface. This probably reflects the increased mechanical strength provided by the carbon support film. Surprisingly, we never found well-ordered single-layered crystals with *p*6 symmetry growing on the carbon films, whereas such crystals seemed to form readily at the air-water interface. This may be an effect of a local increase in the concentration of hexamers on the drop surface which is more rapid in the absence of the carbon film, or of the kinetics of crystal formation, as diffusion on the air-water interface is likely to be faster than on the surface of a solid substrate, even with detergent present. Crystalline monolayers were always less well ordered than the double layers grown at the air-water interface. They were also quite rare and difficult to distinguish from double-layered crystals, except by image processing, and therefore much less suitable for 3D data collection. It is worth noting that some images of 2D crystals at the air-water interface also showed *p*321 projection symmetry, indicating that they were double layers.

The three-dimensional density map (Auer *et al*., 1998) revealed that the two layers are in contact *via* their small extracellular portion, with the large hydrophilic parts of this highly asymmetric membrane protein facing the carbon surface and the solution, respectively. The contact to the carbon surface therefore seems to be mediated by hydrophilic forces, as in the formation of 2D crystals of soluble proteins on lipid monolayers. The crystals have perfect *p*321 symmetry, at least to the resolution to which they diffract, as indicated by the real phases of axial reflections in the 8 Å 3D data set (Auer *et al*., 1998). This means that the two layers have the same structure and that the conformation of the protein is not altered by contact with the substrate.

The formation of double-layered H^+-ATPase 2D crystals can be thought to occur in three stages (Figure 5). Initially, the protein molecules diffuse freely in solution and adsorb to the carbon film. The rate of adsorption of the molecules onto the carbon surface is higher than the rate of desorption, as the hexamers clearly accumulate at the interface. The hexamers then apparently diffuse along the carbon surface and accumulate into a close-packed array. This first single protein layer was found to be non-crystalline, as images taken from such areas indicated poor, if any, order in the Fourier transform. With the formation of a second layer, large crystalline arrays were found, suggesting that the second layer assists in the ordering of the first. As judged by image processing, any additional layers were equally well ordered. Crystallisation on the carbon film was more reproducible and easier to control than on the air-water interface. As the reproducibility of crystallisation experiments often depends on stable crystal nuclei, the carbon film seems to have a favourable effect in protecting the nuclei from disintegrating, as well as providing an interface at which molecules accumulate and rearrange.

The proposed mechanism of crystal formation is consistent with an estimate of the mass thickness of multilayer crystals obtained by low-temperature scanning transmission electron microscopy. These measurements indicated roughly equal mass increments per step from the second layer onwards.

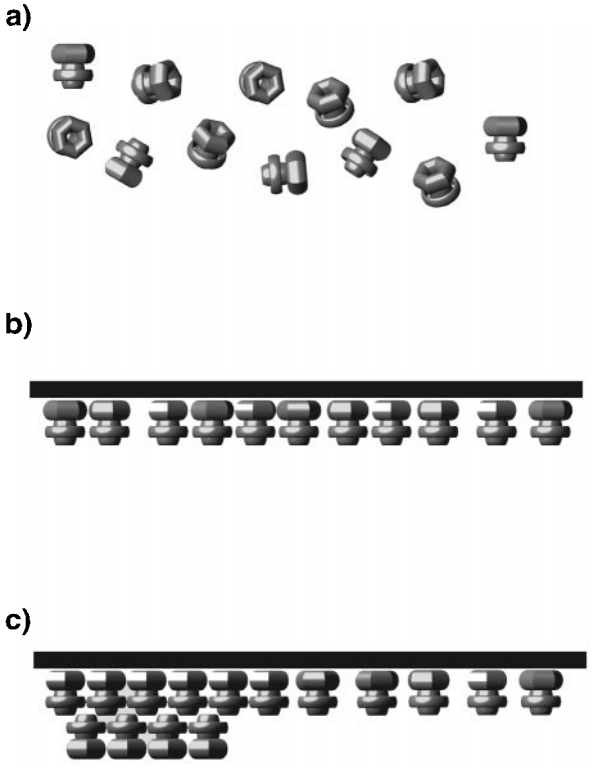

Figure 5. Proposed mechanism for surface crystal formation. (a) Initially, the detergent-solubilised H^+-ATPase diffuses freely in solution. (b) Upon adhesion to the surface, the protein hexamers diffuse along the surface into a close packed, non-crystalline array. (c) Addition of ATPase hexamers in a second layer restricts rotational freedom and locks the molecules of the first layer into a fixed orientation which results in the formation of a 2D crystal with a thickness of two protein molecules and *p*321 symmetry.

The first step, which from image processing is known to be poorly ordered, had a larger mass density than the others, as might be expected of a single layer of hexamers plus a carbon film. As the thickness of each step and of the carbon film is, however, not known in absolute terms, it cannot be ruled out that the 3D crystals form by epitaxial growth in steps of well-ordered double layers on top of a disordered single layer.

Surface-assisted crystallisation has been used in the past to generate 2D crystals of a variety of soluble proteins. Crystalline arrays of F_1-ATPase and ferritin formed at a liquid-liquid interface (Yoshimura *et al.*, 1990; Aoyama *et al.*, 1995), alcohol oxidase was crystallised on carbon-coated formvar film (Vonck & van Bruggen, 1990) and chloroplast F_1-ATPase formed 2D crystals on carbon-coated grids (Boekema & Böttcher, 1992). Various protein assemblies, including the 50 S ribosome, RNA polymerase, and cholera toxin, form extensive 2D crystals on lipid monolayers (see the review by Kornberg & Darst, 1991), and some of these were sufficiently well ordered for structural studies at 6-12 Å resolution. The technique of lipid monolayer crystallisation seems to be unsuitable for membrane proteins, however, as the detergent which is necessary to solubilise the protein would disrupt the lipid monolayer.

The 2D crystals described here are fundamentally different from other 2D crystals of membrane proteins grown by lipid reconstitution and detergent removal, and can be considered as 3D crystals consisting of detergent-protein complexes (Michel, 1982) with a thickness of a single unit cell. Surface crystallisation on a carbon support film resembles the epitaxial growth of 3D crystals on heterologous surfaces, which has been used to crystallise bacteriorhodopsin on benzamidine crystals (Schertler *et al.*, 1993). Unlike 3D crystallisation, however, the formation of 2D crystals is very quick and economical: once crystallisation conditions were established, each experiment required only ~7 µg of protein, most of which could be recovered if necessary, and the result could be assessed by electron microscopy within one to two hours. We hope that surface crystallisation will provide a way to grow 2D crystals for structure determination by electron microscopy for soluble or membrane proteins that can only be obtained in small quantities, especially if 3D crystals can be obtained but their quality or stability is insufficient for high-resolution structure determination by X-ray crystallography.

Methods

Two-dimensional crystals

The 2D crystals were grown on carbon films, supported on thin, gold-plated copper 400 mesh electron microscope grids (Plano) from a solution containing the 1 mg/ml H^+-ATPase, 1.28 mg/ml dodecymaltoside, 0.1 % (w/v) trehalose, 100 mM ammonium sulphate and 10.5 % (w/v) PEG 4000 (Fluka) in a solution containing 30 % (w/v) glycerol, 1 mM EDTA, 1 mM dithiothreitol and 2 µg/ml chymostatin, with the pH being adjusted to 6.8 with Tris (Cyrklaff *et al.*, 1995). Gold-plated grids were used to avoid corrosion of standard Cu grids in contact with the crystallising solution. Carbon-coated grids were heated to 160 °C for one hour prior to the experiment in order to improve the mechanical stability of the carbon film as well as its adhesion to the supporting grid. In a typical crystallisation experiment, a 7 µl drop of the crystallising solution was placed on a siliconised coverslip. The grid was immediately placed onto the drop with the grid bars facing the solution, taking care not to trap air bubbles. The coverslip was inverted onto the well of a Linbro tissue culture plate containing 1 ml of water, sealed with immersion oil (Sigma) and left at 4 °C for one to four hours.

Specimen preparation and electron microscopy

Grids were picked up from the surface of the drops, blotted for five to ten seconds with two to four layers of filter paper (Whatman No. 4) and frozen in liquid ethane (Dubochet *et al.*, 1988). The blotting and freezing pro-

cedure was critical because insufficient blotting left an undesirably thick film of viscous buffer, whereas excessive blotting resulted in drying and loss of crystal order. The frozen grid was transferred at liquid-nitrogen temperature into a Gatan cryotransfer specimen holder and observed at ~100 K in a Philips CM200 FEG or in a JEOL 2000 EX electron microscope operated at 200 kV acceleration voltage. Crystals were located either in defocused diffraction mode (JEOL 2000 EX) or at a magnification of 1500 and high defocus (Philips CM200 FEG). Images for structure determination were recorded at low-dose conditions in a Philips CM200 FEG at a magnification of 50,000 on Kodak SO-163 film and developed for 12 minutes with full-strength Kodak D19.

Image processing

Micrographs were screened by optical diffraction. Areas of 8000 × 8000 pixels were digitised using a Zeiss SCAI scanner with a step size of 7 μm. Images were processed on a DEC/Alpha workstation using the MRC image processing programs (Crowther *et al.*, 1996). Phase comparison of symmetry-related reflections using the program ALLSPACE (Crowther *et al.*, 1996) indicated *p*321 symmetry for crystals with tilt angles of less than 5°, due to their large thickness of ~240 Å (Auer *et al.*, 1998). After two cycles of unbending (Henderson *et al.*, 1986) and correction for the contrast transfer function, a list of amplitudes and phases of structure factors was obtained, and a projection map was calculated with CCP4 software (Collaborative Computational Project No. 4, 1994). The model projection structure of a double-layered *p*321 crystal was calculated from the previously obtained projection *p*6 of crystalline monolayers (Cyrklaff *et al.*, 1995) using the package EM (Hegerl, 1996).

Acknowledgements

We thank Deryck Mills for carrying out the STEM mass measurements. W.K. gratefully acknowledges financial support from the Deutsche Forschungsgemeinschaft. Support to GAS was from USPHS NIH Grant #GM24784. We thank Hans Hebert for his help with the EM program package and our colleagues at EMBL for stimulating discussions.

References

Aoyoma, K., Ogawa, K., Kimura, Y. & Fujiyoshi, Y. (1995). A method for 2D crystallisation of soluble proteins at liquid-liquid interface. *Ultramicroscopy*, **57**, 345-354.

Auer, M., Scarborough, G. A. & Kühlbrandt, W. (1998). Three-dimensional map of the plasma membrane H^+-ATPase in the open conformation. *Nature*, **392**, 840-843.

Boekema, E. J. & Böttcher, B. (1992). The structure of ATP synthase from chloroplasts. Conformational changes of CF1 studied by electron microscopy. *Biochim. Biophys. Acta*, **1098**, 131-143.

Chadwick, C. C., Goormaghtigh, E. & Scarborough, G. A. (1987). A hexameric form of the *Neurospora crassa* plasma membrane H^+-ATPase. *Arch. Biochim. Biophys.* **252**, 348-356.

Cheng, A., v. Hoek, A. N., Yeager, M., Verkman, A. S. & Mitra, A. (1997). Three-dimensional organisation of a human water channel. *Nature*, **387**, 627-630.

Collaborative Computational Project No. 4 (1994). The CCP4 suite: programs for protein crystallography. *Acta Crystallog. sect. D*, **50**, 760-763.

Cowan, S. W., Schirmer, T., Rummel, G., Steiert, M., Ghosh, R., Pauptit, R. A., Jansonius, J. N. & Rosenbusch, J. P. (1992). Crystal structures explain functional properties of two *E. coli* porins. *Nature*, **358**, 727-733.

Crowther, R. A., Henderson, R. & Smith, J. M. (1996). MRC image processing programs. *J. Struct. Biol.* **116**, 9-16.

Cyrklaff, M., Auer, M., Kühlbrandt, W. & Scarborough, G. A. (1995). 2-D structure of the *Neurospora crassa* plasma membrane ATPase as determined by electron cryomicroscopy. *EMBO J.* **14**, 1854-1857.

Deisenhofer, J., Epp, O., Miki, K., Huber, R. & Michel, H. (1984). X-ray structure analysis of a membrane-protein complex: electron-density map at 3 Å resolution and a model of the chromophores of the photosynthetic reaction centre from *Rhodopseudomonas viridis*. *J. Mol. Biol.* **180**, 385-398.

Doyle, D. A., Cabral, J. M., Pfuetzner, R. A., Kuo, A., Gulbis, J. M., Cohen, S. L., Chait, B. T. & MacKinnon, R. (1998). The structure of the potassium channel: molecular basis of K^+ conduction and selectivity. *Science*, **280**, 69-77.

Dubochet, J., Adrian, M., Chang, J.-J., Homo, J.-C., Lepault, J., McDowall, A. W. & Schultz, P. (1988). Cryo-electron microscopy of vitrified specimens. *Quart. Rev. Biophys.* **21**, 129-228.

Hegerl, R. (1996). The EM package: a platform for image processing in biological electron microscopy. *J. Struct. Biol.* **116**, 30-34.

Henderson, R. (1995). The potential and limitations of neutrons, electrons and X-rays for atomic resolution microscopy of unstained biological molecules. *Quart. Rev. Biophys.* **28**, 171-193.

Henderson, R., Baldwin, J. M., Downing, K. H., Lepault, J. & Zemlin, F. (1986). Structure of purple membrane from *Halobacterium halobium*: recording, measurement and evaluation of electron micrographs at 3.5 Å resolution. *Ultramicroscopy*, **19**, 147-178.

Henderson, R., Baldwin, J. M., Ceska, T. A., Zemlin, F., Beckmann, E. & Downing, K. H. (1990). Model for the structure of bacteriorhodopsin based on high-resolution electron cryomicroscopy. *J. Mol. Biol.* **213**, 899-929.

Iwata, S., Ostermeier, C., Ludwig, B. & Michel, H. (1995). Structure at 2.8 Å resolution of cytochrome c oxidase from *Paracoccus denitrificans*. *Nature*, **376**, 660-669.

Jap, B., Zulauf, M., Scheybani, T., Hefti, A., Baumeister, W., Aebi, U. & Engel, A. (1992). 2D crystallisation: from art to science. *Ultramicroscopy*, **46**, 45-84.

Koepke, J., Hu, X., Muenke, C., Schulten, K. & Michel, H. (1996). The crystal structure of the light-harvesting complex II (B800-850) from *Rhodospirillum molischianum*. *Structure*, **4**, 581-597.

Kornberg, R. D. & Darst, S. A. (1991). 2D crystals of proteins on lipid layers. *Curr. Opin. Struct. Biol.* **1**, 642-646.

Kühlbrandt, W. (1992). Two-dimensional crystallisation of membrane proteins. *Quart. Rev. Biophys.* **21**, 429-477.

Kühlbrandt, W., Wang, D. N. & Fujiyoshi, Y. (1994). Atomic model of plant light harvesting complex by electron crystallography. *Nature,* **367**, 614-621.

Li, H., Lee, S. & Jap, B. (1997). Molecular design of aquaporin-1 water channel as revealed by electron crystallography. *Nature Struct. Biol.* **4**, 263-265.

McDermott, G., Prince, S. M., Freer, A. A., Hawthornthwaite-Lawless, A. M., Papitz, M. Z., Cogdell, R. J. & Isaacs, N. W. (1995). Crystal structure of an integral membrane light-harvesting complex from photosynthetic bacteria. *Nature,* **374**, 517-521.

Michel, H. (1982). Three-dimensional crystals of a membrane protein complex. The photosynthetic reaction centre from *Rhodopseudomonas viridis*. *J. Mol. Biol.* **158**, 567-572.

Pebay-Peroula, E., Rummel, G., Rosenbusch, J. P. & Landau, E. M. (1997). High resolution X-ray structure of bacteriorhodopsin from microcrystals grown in lipidic cubic phases. *Science,* **277**, 1676-1680.

Rigaud, J.-L., Mosser, G., Lacapere, J.-L., Olofsson, A., Levi, D. & Ranck, J.-L. (1997). Bio-Beads: an efficient strategy for two-dimensional crystallisation of membrane proteins. *J. Struct. Biol.* **118**, 226-235.

Scarborough, G. A. (1994). Large single crystals of the *Neurospora crassa* plasma membrane H^+-ATPase: an approach to the crystallisation of integral membrane proteins. *Acta Crystallog. sect. D,* **50**, 643-649.

Schertler, G. F. X. (1993). Orthorhomic crystal form of bacteriorhodopsin nucleated on benzamidine diffracting to 3.6 Å resolution. *J. Mol. Biol.* **234**, 156-164.

Song, L., Hobaugh, M. R., Shustak, C., Cheley, S., Bayley, H. & Gouaux, J. E. (1996). Structure of staphylococcal α-hemolysin, a heptameric transmembrane pore. *Science,* **274**, 1859-1866.

Tsukihara, T., Aoyama, H., Yamashita, E., Tomizaki, T., Yamaguchi, H., Shinzawa-Itoh, K., Nakashima, R., Yaona, R. & Yoshikawa, S. (1995). Structure of metal sites of oxidised bovine heart cytochrome c oxidase at 2.8 Å. *Science,* **269**, 1069-1074.

Unger, V. M., Hargave, P. A., Baldwin, J. M. & Schertler, G. F. X. (1997). Arrangement of rhodopsin transmembrane alpha-helices. *Nature,* **389**, 203-206.

Unwin, P. N. T. (1995). Acetylcholine receptor channel imaged in the open state. *Nature,* **373**, 37-43.

Vonck, J. & van Bruggen, E. F. J. (1990). Electron microscopy and image analysis of two-dimensional crystals and single molecules of alcohol oxidase from *Hansenula polymorpha*. *Biochim. Biophys. Acta,* **1038**, 74-79.

Walz, T., Hirai, T., Murata, K., Heymann, J. B., Mitsuoka, K., Fujiyoshi, Y., Smith, B. L., Agre, P. & Engel, A. (1997). The three-dimensional structure of aquaporin-1. *Nature,* **387**, 624-627.

Weiss, M. S., Abele, U., Weckesser, J., Welte, W., Schiltz, E. & Schulz, G. E. (1991). Molecular architecture and electrostatic properties of a bacterial porin. *Science,* **254**, 1627-1630.

Yoshimura, H., Matsumoto, M., Endo, S. & Nagayama, K. (1990). Two-dimensional crystallisation of proteins on mercury. *Ultramicroscopy,* **32**, 265-274.

Yu, C. A., Xia, J. Z., Kachurin, A. M., Yu, L., Xia, D., Kim, H. & Deisenhofer, J. (1997). Crystal structure of beef heart mitochondrial cytochrome-bc_1 complex. *Science,* **277**, 1136-1144.

Zhang, P., Toyoshima, C., Yonekura, K., Green, N. M. & Stokes, D. L. (1998a). Structure of the calcium pump from sarcoplasmic reticulum at 8 Å resolution. *Nature,* **392**, 835-839.

Zhang, Z., Huang, L., Shulmeister, V. M., Chi, Y.-I., Kim, K. K., Hung, L.-W., Crofts, A. R., Berry, E. A. & Kim, S.-H. (1998b). Electron transfer by domain movement in cytochrome bc_1. *Nature,* **392**, 677-684.

Edited by M. F. Moody

(Received 21 August 1998; received in revised form 18 February 1999; accepted 18 February 1999)